Environmental Consequences of Nuclear War Volume I:
Physical and Atmospheric Effects
A. B. Pittock, T. P. Ackerman, P. J. Crutzen,
M. C. MacCracken, C. S. Shapiro and R. P. Turco

CHAPTER 3

Sources and Properties of Smoke and Dust

3.1 INTRODUCTION

Recent studies have emphasized the large changes in atmospheric optical, meteorological, and chemical conditions that can result from fires started during a nuclear war (Crutzen and Birks, 1982; Turco et al., 1983a,b; Crutzen, Galbally and Brühl, hereafter CGB, 1984; NRC, 1985). In particular, attention has been focused on the effects of smoke formed in flaming combustion. This smoke has high concentrations of amorphous elemental carbon which strongly absorbs solar radiation. In this chapter, estimates are made of the quantities of smoke that might be produced by both urban/industrial and wildland fires started by a nuclear war such as described in Chapter 2. The microphysical and optical properties of the particles which comprise the smoke are also discussed and estimates of the attenuation of sunlight by the smoke are made. A brief discussion of dust raised by surface bursts is also included. Finally, the related, but special, issue of urban fire spread and urban fire modelling is included in an Appendix.

3.2 THE ORIGIN OF SMOKE IN COMBUSTION

Smoke is formed from the burning of organic materials. The burning process can be conveniently differentiated into two phases: high-temperature, flaming combustion during which sooty smoke is formed, and low-temperature, smoldering combustion during which primarily hydrocarbons are formed. The sooty smoke is of greater significance for the atmospheric radiation balance because such smoke absorbs sunlight very efficiently. Smoldering combustion, on the other hand, produces an aerosol that predominantly scatters rather than absorbs sunlight.

In flames, temperatures are sufficiently high that organic molecules can lose a large fraction of their hydrogen atoms by pyrolysis, leading to radical and ionic molecules with high C/H ratios. The free hydrogen which is created

may be oxidized or may escape to the atmosphere. These soot precursors condense into hexagonal crystallites with dimensions on the order of 1 to 5 nm, which then grow further into embryonic amorphous elemental carbon spheroids with radii of the order of a few tens to a hundred nanometers and an average C-to-H atomic ratio of about 10 to 1. If these soot spheroids escape the flame, they cannot be oxidized further since oxidation requires temperatures above about 1500 K (Gaydon and Wolfhard, 1970; Wagner, 1980). Outside the flames, these carbon spheroids can aggregate into chain-like structures, sometimes consisting only of a few spheroids, sometimes forming fluffy agglomerates up to 100 μm in size (Russell, 1979; Day et al., 1979; Bigg, 1985). The surface to mass ratio of the agglomerates, however, remains relatively constant, as they grow in size.

Since in actual fire situations combustion is often not complete, the soot and smoke particles that are emitted into the atmosphere contain a substantial fraction of unburned organic matter. Soot is, therefore, a complex mixture mainly consisting of amorphous elemental carbon and oily material. Generally, smokes with higher elemental carbon contents appear blacker.

The smoke yield (defined as the mass of smoke produced per mass of material burned) and the elemental carbon fraction of the smoke are strongly dependent on the nature of the fuel and the mode of burning. Partly oxidized wood (e.g., forest materials and construction wood) produces much less elemental carbon than fossil fuel and fossil fuel-derived products. Smoldering combustion produces virtually no elemental carbon because temperatures are too low for hydrocarbon dehydrogenation to occur. Estimates of smoke yields and elemental carbon fractions for various combustible materials are given in the following sections.

3.3 SMOKE EMISSIONS FROM URBAN/INDUSTRIAL FIRES

The difficulties and uncertainties in estimating the smoke emissions from a single, large urban fire are very great. The first problem is to estimate the quantity of combustible material available and the fraction of that material that will burn. The latter factor is a complicated function of the fuel loading and type, the behavior of mass fires in urban areas, and the meteorological conditions which exist at the time of burning. Furthermore, quantitative information on smoke and amorphous elemental carbon production from fires in various materials is still limited and mainly available from test fires that were conducted under controlled laboratory conditions with small quantities of combustible material. Consequently, there is a question about the applicability of these data to mass fire conditions. The smoke emission problem is compounded when the effects of a hypothetical nuclear war are considered, due to the large number of possible urban and industrial targets. Some of the problems associated with selecting a scenario for a nuclear war,

including the extent to which urban and industrial complexes and fossil fuel storage facilities are targeted, were discussed in Chapter 2. Estimating the smoke emission from fires ignited in the vicinity of these various targets is made more difficult by the variability in fuel loadings and types and in the prevailing meteorological conditions.

Quantitative information from mass fires is largely lacking despite several examples of large city fires during the Second World War, including those following the nuclear attacks on Hiroshima and Nagasaki. Studies of the destruction of Nagasaki and Hiroshima show that essentially complete burnout occurred wherever the thermal energy fluence from the nuclear explosions exceeded 20 and 7 cal/cm^2 respectively. No quantitative information is available on the smoke production caused by these fires.

Despite the substantial difficulties and uncertainties involved, three studies have attempted to make some estimates of smoke production from fires in a nuclear war (Turco et al., 1983a,b; NRC, 1985; CGB, 1984). The results from the studies by Turco et al. (1983a) and the NRC (1985) are very similar. Therefore, the following discussion will concentrate on a comparison of the NRC and CGB studies.

3.3.1 Urban Areas and Combustible Burdens

In both the NRC and CGB studies, it was assumed that a nuclear heat pulse of at least 20 cal/cm^2 is required for mass fires to occur in cities. This may be a conservative assumption, as only 7 cal/cm^2 reached the perimeter of the burnout area in Hiroshima (Glasstone and Dolan, 1977). In fact, the NRC report mentions that, even in Nagasaki, in directions unobscured by hills, total burnout occurred at all sites where the heat pulse exceeded about 10 cal/cm^2 (see Chapter 1 of this Volume for further discussion). The potential fire area per megaton of explosive yield, roughly corresponding to the 20 cal/cm^2 irradiation zone, were taken to be 250 km^2/Mt by Turco et al. (1983a) and by the NRC and 375 km^2/Mt by CGB. These area per Mt estimates were used both for urban and wildland fires.The values differ somewhat because of differences in assumptions about atmospheric visibility, overlap of fire zones, and fire spread. In many urban fire situations, firespread would be expected to contribute significantly to the total fire area (see Appendix 3A), thus increasing the area burned per Mt. Both the area estimates given above appear to be conservative for isolated bursts if a burnout criterion of 10 cal/cm^2 is adopted. This latter value of the fluence corresponds roughly to that experienced at Hiroshima and Nagasaki, for which equivalent fire areas of 300 to 1200 km^2/Mt occurred (see Chapter 1).

A weapon yield of 0.4 Mt corresponds approximately to the average yield of nuclear weapons that might be used in attacks on targets located near or in cities (see Table 2.1, Chapter 2). In the NRC study it was assumed

that a total yield of 1500 Mt of nuclear weapons, out of a total of 6500 Mt, might be used against military command and industrial targets that are co-located near or in large cities in the Warsaw Pact and NATO countries. Taking into account a factor of 1.5 overlap of potential fire areas, a total urban area of 0.25×10^6 km^2 was assumed to burn, which corresponds to about half of the area of the 1000 cities with more than 100,000 inhabitants in both combatant blocks (Turco et al., 1983b; NRC, 1985). In the CGB scenario, 300 of the most important urban industrial centers of the NATO and Warsaw Pact nations were assumed to be targeted with about 800 Mt of nuclear weapons, each having an average yield of 0.4 Mt. Allowing for a factor of three overlap between potential fire areas, the corresponding total urban area in the CGB study is likewise about 0.25×10^6 km^2. It is estimated that the number of potential human casualties in the destroyed cities would be about 250 million, which is 30% of the total urban population in the combatant nations (UN, 1980b).

TABLE 3.1.
POPULATION AND NUMBER OF CITIES IN THE DEVELOPED WORLD IN GIVEN SIZE CLASSES (UN, 1980B)

Size class (millions)	Number of cities	Total population (millions)
>4	16	142
2–3.9	27	73
1–1.9	74	99
Sum	117	314
Total urban		834

The urban population of the industrialized nations is between 65 and 75% of the total population of these nations (UN, 1980b). Statistics on the populations of the largest cities in the developed world are given in Table 3.1. These statistics indicate that 40% of the total urban population live in the largest 120 industrial and commercial centers of the combatant nations. The total destruction of all of these urban areas, therefore, implies the potential burning of at least 40% of all processed combustible materials in the NATO and Warsaw Pact nations. Katz (1982) estimated that attacks with 600 warheads carrying a total of 300 Mt of nuclear weapons could destroy up to 60% of all U.S. industry and 40% of its population. An analysis of the U.S.S.R. population distribution and industrial capacity (Kemp, 1974) showed that the largest 50 cities contained 33% of the urban population and 40% of the industrial capacity.

According to the 1980 U.S. Census, about half of the total U.S. population lives in the 62 largest metropolitan centers. Of these urban dwellers, about

50% live in about 10% of the total developed areas. This implies that urban combustibles are concentrated in relatively small areas. Hence, the total built up area that might be subject to direct or collateral damage in a nuclear war is of great importance with regard to the quantification of the combustible material which might burn. In some cases, the cores of the central cities provide sufficient fuel loading to support "firestorm" conditions that might lift smoke to the upper troposphere and lower stratosphere (see Appendix 3A and Chapter 4). As pointed out by Turco et al. (1983a), the complete burning of a hundred large population and commercial centers could, within the range of current uncertainties, produce about as much smoke and soot as that estimated in the baseline cases which were adopted by Turco et al. (1983a), NRC (1985) and CGB (1984).

An important element of these studies is the need to estimate explicitly the amounts of combustible material in the urban and industrial centers. Here the NRC and CGB studies followed different approaches. Using the limited information available from surveys of U.S. cities by FEMA (1982) and statistics on the world production of combustible materials, the NRC study adopted an average combustible material loading of 40 kg/m^2 in urban areas, representing a weighted mean between heavy loading of the order of several hundred kg/m^2 in the cores of cities and a much lighter loading down to 5 kg/m^2 in the suburbs. This leads to an estimated total of ten thousand million tonne (10^{16} g) of material that could be consumed in fires. Three quarters of this, or 7.5 thousand million tonne (7.5×10^{15} g), was assumed to burn (NRC, 1985). This quantity of combustibles was assumed to consist of 5 thousand million tonne (5×10^{15} g) wood, 1.5 thousand million tonne (1.5×10^{15} g) liquid fossil fuels, and one thousand million tonne (10^{15} g) of industrial organochemicals, plastics, polymers, rubber, resins, etc.

The CGB estimates were made differently. Material production statistics in the developed world were assembled from the United Nations and other sources, as reproduced in Table 3.2. Based on these data and the assumed average lifetimes of wood in constructions and furnishings, CGB estimated that the urban centers that would be targeted could contain about 4000 million tonne (4×10^{15} g) of cellulosic materials in constructions, furnishings, plywood, books, etc. This amount is about equal to 25% of all available cellulosic materials in the developed world, and about 35% of all such materials in the urban centers of these countries. It was assumed that half of this, i.e., 2000 million tonne (2×10^{15} g), would burn in flaming combustion (see Appendix 3A). The remaining material would not burn, or would smolder over days to weeks (see also Chandler et al., 1963). Since our primary concern here is the sooty smoke that is produced by flaming combustion, only the 2×10^{15} g of cellulosic materials that would burn quickly will be considered. In Chapter 6, the potential chemical effects of the smoke produced by smoldering fires will be discussed.

TABLE 3.2
ANNUAL PRODUCTION OF VARIOUS COMBUSTIBLE MATERIALS AND ESTIMATED ACCUMULATED QUANTITIES IN DEVELOPED WORLD (SEE TEXT, AND UN, 1980B; 1981; FAO, 1976; WORLD BANK, 1978). FOR FOODSTUFFS, ONLY STORAGE IN URBAN AREAS WAS CONSIDERED (SEE VOLUME II)

Material	Production (g/y)	Accumulation (g)
Liquid fuels	3.1×10^{15}	$1.1–1.5 \times 10^{15}$
Coal, lignite	3.5×10^{15}	$\sim 10^{15}$
Natural gas and liquids	8.9×10^{14}	1.5×10^{14}
Sawnwood, panels, etc.	3.4×10^{14}	1.4×10^{16}
Pulp, paper, paperboard	9×10^{14}	$\sim 10^{15}$
Bitumen, total	(7×10^{13})	$(1–1.5 \times 10^{15}$ g)
roof protection	10^{13}	$\sim 2 \times 10^{14}$
city roads	3×10^{13}	6×10^{14}
Organic polymers	(7×10^{13})	(4.6×10^{14})
plastics	4×10^{13}	2×10^{14}
resins and paint	1.2×10^{13}	1.2×10^{14}
fibers	1.4×10^{13}	1.4×10^{14}
Cotton	10^{13}	10^{14}
Fats and oils	7×10^{13}	2×10^{13}
Cereals	3×10^{14}	$0.5–2 \times 10^{14}$
Sugar	5×10^{13}	2×10^{13}

CGB included fossil fuel and fossil fuel-derived products as a separate category of combustibles and showed that combustion of these materials most likely would have the gravest potential optical effects. According to information supplied by the Oil Market Division of the OECD in Paris, the total oil stocks at the primary level in ports and refineries in OECD countries in 1984 were equal to 420 million tonne (4.2×10^{14} g), including 70 million tonne (7×10^{13} g) of strategic stocks in the U.S., West Germany, and Japan. Underground storage of oil amounts only to 60 million tonne (6×10^{13} g), mainly in the U.S. and West Germany. At the distributor and user level, additional stocks of petroleum and petroleum-derived fuels vary between 40% and 100% of those at the primary level. The quantity of oil at sea is about 100 million tonne (10^{14} g). The OECD countries represent about 60% of the total world oil trade. From this information, CGB estimated, therefore, that the total amount of oil that is currently stored in the developed world is in the range of 1.1–1.5 thousand million tonne ($1.1–1.5 \times 10^{15}$ g). About one thousand million tonne (10^{15} g) might be readily available for burning following attacks on targets co-located with urban areas. To this must be added similarly large quantities of coal stockpiled at mines, power stations, and elsewhere, although the ignition and free burning of coal is probably less significant.

About 70 million tonne (7×10^{13} g) of the annual crude oil production goes into asphalt production (UN, 1981). An analysis of the bitumen production (UN, 1981) indicates that 1.0–1.5 thousand million tonne (1.0–1.5×10^{15} g) bitumen has accumulated in the developed world. The flaming point of bitumen is between 210 and 290°C (Güsfeldt, 1974), so that this material can readily burn in intense fires. In West Germany almost 30% of the bitumen is now used in the building construction industry, including 15% for roof insulation purposes (Arbeitsgemeinschaft der Bitumen-Industrie, personal communication). In the U.S., the proportion is about 19% (B. Williamson, personal communication). The rest of the bitumen has been applied on roads and highways. The urban fraction of this in West Germany is about 60% (Arbeitsgemeinschaft der Bitumen-Industrie, personal communication). This implies that together about 700 million tonne (7×10^{14} g) of bitumen might be available for burning in the urban areas of the developed world. Of this quantity, the nearly 200 million tonne (2×10^{14} g) of bitumen on roofs would be particularly easy to burn.

The world production of petroleum-derived organic polymers in 1980 amounted to about 60 million tonne (6×10^{13} g) (UN, 1981; Weissermel and Müller, 1981). Extrapolating from West German conditions, the synthesis of polymers from natural gas as the feedstock adds another 10 million tonne (10^{13} g) of organic polymers to the 1980 production figure (Hofmann and Krauch, 1982). The total of 70 million tonne (7×10^{13} g) went mainly into the production of 40 million tonne (4×10^{13} g) of plastics, 12 million tonne (1.2×10^{13} g) of synthetic resins and paints, and 14 million tonne (1.4×10^{13} g) of synthetic fibers (UN, 1981; Hoechst A.G., private communication). Assuming average lifetimes of these products of 5, 10, and 10 years, respectively, the amount of stored organic polymers in the developed world could be equal to about 400 million tonne (4×10^{14} g), indicating a ratio of about 1 to 10 between synthetic organic polymers and wood products. According to information from Verband der Sachversicherer (personal communication) the ratio of these products in West Germany is in the range of 1 to 10 or 20 and growing. There are also many additional, individually smaller quantities of materials, such as foodstuffs (W. Cropper, personal communication; see also Volume II of this report) and rubber, that are stored in the developed world. These are summarized in Table 3.2. The total may add up to a hundred million tonne (10^{14} g).

According to the above analysis, in the developed world a total of about 140 million tonne (1.4×10^{14} g) mainly bitumen and synthetic organic polymers, go each year into long-lived products. This compares well with the estimated annual production of 170 million tonne (1.7×10^{14} g) of slowly oxidizing fossil fuel products of Marland and Rotty (1983).

CGB assumed in their calculations that about 700 million tonne (7×10^{14} g) of fossil fuel and fossil fuel derived products might burn in

a nuclear war. This is about 25–30% of the materials readily available for combustion in this category of fuels, excluding coal. The actual amount would, of course, depend on the adopted nuclear war scenario. Nevertheless, because fossil fuel processing facilities and storage depots themselves are likely targets in the case of a major nuclear confrontation (OTA, 1979; see also Chapter 2), the assumption that 700 million tonne (7×10^{14} g) of fossil fuel and fossil fuel derived materials might burn in a major nuclear war seems entirely plausible and serves as a reasonable working hypothesis. Because about half of the available fuel in this category has accumulated in densely populated Europe, a nuclear war limited to this region alone could lead to the hypothesized fuel combustion if 50% of the available fuel were to burn.

The information contained in this section may be summarized as follows. NRC (1985) estimated that altogether 7.5 thousand million tonne of combustibles could burn as a result of a nuclear war. Of this amount, two-thirds were assumed to be wood and wood products, and one-third to be fossil fuel and fossil fuel products. CGB (1984) assumed that 25–30% of all available combustible materials in the developed world would burn, leading to the flaming combustion of two thousand million tonne of wood and wood products, and 700 million tonne of fossil fuel and fossil fuel derived products. From the information given in this section, the burning of these quantities of material could be achieved by nuclear attacks that burned essentially all of less than one hundred of the most important industrial and commercial centers of the developed world.

3.3.2 Smoke Emission Factors

In the NRC study, the average smoke emission factor for all fires was set at about 4% (0.04 g smoke emitted per g fuel), which is the weighted mean of two-thirds cellulosic materials with an emission factor of 3% and one-third liquid fuels and synthetic organics with an emission factor of 6%. The average elemental carbon content of the smoke was taken to be about 20%, which was considered to be a conservative assumption. As a baseline, the NRC study derived total smoke and elemental carbon emissions of about 300 million tonne (3×10^{14} g) and 60 million tonne (6×10^{13} g), respectively. It was assumed that 50% of the smoke would be promptly removed by precipitation in the fire plume, implying net emission values of 150 million tonne (1.5×10^{14} g) for smoke and 30 million tonne (3×10^{13} g) for elemental carbon.

In the study of CGB, smoke emission factors based on the data in Tables 3.3–3.5, were taken to be 1.5% for construction wood, 7% for fossil fuel and asphalt, and 5% for plastics. The corresponding elemental carbon contents were 33, 70, and 80%, respectively. The total estimated smoke emission

from urban fires was then 80 million tonne (8×10^{13} g), of which 45 million tonne (4.5×10^{13} g) was elemental carbon. The largest single contribution to the elemental carbon total is from fossil fuel burning. CGB assumed that one-third of the smoke would immediately rain out in the convective fire columns, leading to the net injection into the background atmosphere of 53 million tonne (5.3×10^{13} g) of smoke, containing 30 million tonne (3×10^{13} g) of elemental carbon.

TABLE 3.3.
LITERATURE SURVEY ON CHARACTERISTICS OF AEROSOL PRODUCED BY BURNING OF WOOD (FROM CRUTZEN, ET AL. 1984). REPRODUCED BY PERMISSION OF D. REIDEL PUBL. COMPANY

Ref. No.	Type	Aerosol yield	Elemental C	Extinction m^2/g fuel
1	Fireplace, softwood	9 g/kg	33% of aerosol	
	Fireplace, hardwood	10 g/kg	8% of aerosol	
2	Residential wood		13% of aerosol	
3	Test fires		50% soot	
	free burning			0.023
	ventilation controlled			0.15
4	Test fires			
	hardwood	0.085–0.16%		
	fiberboard	0.75%		
5	Test fires	1.0–2.5% (flaming) 3.1–16.5% (nonflaming)		
6	Test fires	1.5%	40% of aerosol	0.11
7	Test fires	0.2–0.6%		
"Average"		1.5%	33%	(0.10)

References:

1. Muhlbaier-Dasch, 1982;
2. DeCesar and Cooper, 1983;
3. Rasbash and Pratt, 1979, and private communication D.J. Rasbash;
4. Hilado and Machado, 1978;
5. Bankston et al., 1981;
6. Tewarson, private communication;
7. Seader and Einhorn, 1976.

The estimated emissions of amorphous elemental carbon in the baseline NRC and CGB studies are, therefore, equal, although more smoke is emitted in the NRC scenario. As will be discussed in section 3.6, the climatic effects of nuclear war are mainly determined by the emissions of the strongly

TABLE 3.4.
LITERATURE SURVEY ON CHARACTERISTICS OF AEROSOL PRODUCED IN OIL AND GAS BURNING. NOTE THAT REFERENCES 1–4 ALL REFER TO CLEAN BURNING IN HOUSEHOLD EQUIPMENT AND ARE NOT REPRESENTATIVE FOR FREE BURNING (FROM CRUTZEN ET AL., 1984). REPRODUCED BY PERMISSION OF D. REIDEL PUBL. COMPANY

Ref. No.	Type	Elemental C	Extinction m^2/g fuel
1	Residual oil in burner	31% of aerosol carbon	
2	Diesel engine	80% of aerosol	
	Gas furnace	90% of aerosol carbon	
3	Light oil in burner	40–70% of aerosol	
	Natural gas furnace	40–70% of aerosol	
4	Light oil in burner	40% of aerosol carbon	
5	Oils, rubber	100% soot	0.7–1.2
6	Oil slick	2–6% of fuel burned	
7	Natural gas diffusion flames	all emissions as soot	3
	Heavy fuel oil diffusion flames	all emissions as soot	2
8	Aliphatic oils	3–10% of fuel burned	
9	Benzene, styrene		0.8
"Average"		5% of fuel burned	(0.7)

References:
1. Cooper and Watson, 1979;
2. Muhlbaier-Dasch and Williams, 1982;
3. Nolan, 1979;
4. Wolff et al., 1981;
5. Rasbash and Pratt, 1979; Rasbash, private communication;
6. Day et al., 1979;
7. Maraval, 1972;
8. Rubber and Plastics Research Association of Great Britain, letter to authors;
9. Tewarson, private communication.

light-absorbing elemental carbon. Thus, the climatic consequences of the estimated emissions, which are discussed in the following two chapters, will be similar regardless of whether the NRC or CGB scenario is used.

It is clear from the information gathered in Tables 3.3–3.5 that, even for simple test fires, there is at least a factor of two uncertainty in the smoke and elemental carbon emission yields for each category of combustibles. Further uncertainties are connected with the applicability of this smoke emission data to the mass fires which could develop in large cities in a major nuclear war situation. Various factors, such as the greater intensity of the large fires and the generation of strong convective motions that could loft

TABLE 3.5.
LITERATURE SURVEY ON CHARACTERISTICS OF AEROSOL PRODUCED BY BURNING OF PLASTICS (FROM CRUTZEN ET AL., 1984). REPRODUCED BY PERMISSION OF D. REIDEL PUBL. COMPANY

Ref. No.	Type	Aerosol	Elemental C	Extinction m^2/g fuel
1	Plastics		100% soot	0.2–1.6
	Rubber			1.0
2	Various plastics	5–50% soot	2–40% of fuel	
3	Polyethylene, styrene			
	P.V.C. (flaming)	1.2–3.2%		
	Polyurethane (flaming)	9%		
4	Plastics	6–20%		
5	Plastics	3–5%	100% soot	
6	Plastics	11–20%	75% soot	
7	Plastics			0.3–1.2
8	Automobile components	5%		
9	Plastics		60–100%	
10	Polystyrene	3–10% soot		
	Polyethylene	5–8.3%		
	Polyisoprene	19.4%		
	Polystyrene	21.0%		
11	Various plastics	6.4–9%		0.2–1.7
"Average"		5%	80%	(0.6)

References:
1. Rasbash and Pratt, 1979, and D.J. Rasbash, private communication;
2. Morikawa, 1980;
3. Bankston et al.,1981;
4. Hilado and Machado, 1978;
5. J.E. Snell, private communication;
6. Tewarson et al., 1981;
7. Tewarson, 1982;
8. EPA,1978;
9. Seader and Ou, 1977;
10. Rubber Plastics Research Association of Great Britain, letter to authors;
11. Tewarson, private communication.

debris, argue for larger emission factors in the case of the large fires. There are strong indications that ventilation-controlled fires produce much more smoke than free burning test fires (e.g. Rasbash and Pratt, 1979). Also, in a nuclear war, much of the burning of liquid fuels would occur from ruptured fuel containers which would create pool fires. These fires and the burning of street asphalt may produce substantially more than 7% smoke (Rasbash, private communication). High coagulation rates in the dense smoke plumes of oil fires might lead to fluffy soot particles in the supermicron range. (The

microphysical and optical properties of these large particles are discussed below.) It is also possible that in large pool fires an appreciable fraction of the oil would be volatilized without burning and then condense as oil droplets a few millimeters in size; such large drops would be removed rapidly from the atmosphere by gravitational settling. Observations of the size and optical properties of the aerosol generated in large oil fires are, unfortunately, not available, leaving this as one of the most critical sources of uncertainty in the estimates of smoke emission. Further research on the emissions from large fires is clearly needed (see Chapter 8).

3.4 PARTICULATE EMISSIONS FROM FOREST AND WILDLAND FIRES

Both the NRC (1985) and the CGB (1984) studies considered as baseline cases that 0.25×10^6 km^2 of forest could burn in a nuclear war. The NRC study assumed that on a purely random basis about 40% of the attacks on military targets could occur above forests and 40–50% over brushlands and grasslands. According to a meteorological analysis by Huschke (1966), about 50% of such areas are medium to highly flammable during the summer. Because effective fire fighting would not be possible during and after a nuclear war, such forest areas, once ignited, could spread over larger areas than what is now normally the case. Assuming that fires would burn over all areas receiving thermal pulses larger than 20 cal/cm^2, corresponding to a fire area of 250 km^2/Mt, the total forest area that could burn during summer and fall would be equal to 250,000 km^2, if neither overlap of fire areas nor fire spread are considered. In an alternative calculation the NRC panel considered the effects of attacks on missile silo fields (2000 Mt) and other military targets (3000 Mt).The missile silo fields occupy an area of 250,000 km^2, of which it was estimated that 50,000 km^2 were located in forested areas. It was assumed that this entire forest area would be totally incinerated. The remaining 3000 Mt on military targets could lead to fires in 150,000 km^2 of forest. According to NRC, if some fire spread is considered, a total of 250,000 km^2 of forest could burn in a nuclear war.

In the CGB study, which was based on the Ambio scenario, it was assumed that a statistical average of 22% of the total megatonnage used in the war (i.e., 1000 Mt) would explode on forest lands and 43% in brushlands and grasslands (Galbally et al., 1983). Prominent among the targets are ICBM silos that receive two 0.5 Mt weapons per site and, altogether, 70% of the total megatonnage (about 2000 Mt). The average spacing between Minuteman silos in the U.S. corresponds to an average area around each silo of about 100–150 km^2. If such close spacing also applies in the U.S.S.R., the area of forest burning near ICBM sites could be no more than 50,000 km^2.

The remaining 30% of the megatonnage (about 900 Mt) would consist of 0.2–0.3 Mt weapons, used mainly against single military targets, such as army and air bases and command posts. Extrapolating from data quoted by Hill (1961) which include estimates of firespread, the minimum fire spread area for a 0.25 Mt weapon would be 200 km^2. With about 1400 explosions, it was, therefore, concluded that 200,000 km^2 of forest land could burn near military targets other than ICBM silos. Considering that additional forest fires could start near cities and industries, a forest fire area of 500,000 km^2, according to CGB, would be possible. The total forest fire area estimated by CGB would have been appreciably reduced to 100,000 km^2 if a more conservative burnout criterion of 250 km^2/Mt, which neglects firespread, had been adopted.

The average load of combustibles in temperate forests is about equal to 20 kg/m^2, of which it was assumed that about 20% could be consumed by the fires. This assumption is somewhat larger than in normal forest fires (Safronov and Vakurov, 1981), but takes into account the effects of simultaneous ignitions, which could lead to mass fires, and debris formation by nuclear blasts. These figures lead to a total forest fuel consumption of 10^{15} g, as calculated by both NRC and CGB, for a total forest fire area of 250,000 km^2. On the average, half of the fuel would be consumed in flaming and half in smoldering combustion (Chandler et al., 1963; Wade, 1980). The smoldering combustion produces about 5 times more particulate matter than flaming combustion (Wade, 1980). Based mostly on the compilations by Ward et al. (1976), the smoke emission factor (mass of smoke produced per mass of fuel) was assumed to be 3% in the NRC study and 6% in the CGB study. Of this, 10% was assumed to be amorphous elemental carbon. This leads to total smoke and elemental carbon emissions of 3×10^{13} g and 3×10^{12} g (NRC, 1985) and 6×10^{13} g and 6×10^{12} g (CGB, 1984), respectively. These quantities are appreciably smaller than the potential smoke emissions from urban and industrial targets.

Some recent studies indicate that the effects of forest fires may have been overestimated in the NRC and CGB studies. Patterson and McMahon (1984) inferred elemental carbon fractions ranging from 0.5 to 20% from light absorption measurements in smoke produced from forest fuels in laboratory experiments. As expected, the smaller values were associated with smoldering combustion and the larger with flaming combustion. Emission factors for the flaming fires were found to be between 0.8 and 2%, and for the smoldering fires were about 5 to 6%. In combination, these factors gave estimated elemental carbon emission factors from laboratory pine needle fires ranging from 0.07 to 0.25%. In considering data from low-intensity field burns with forest fuels, Patterson and McMahon (1985a,b) inferred an elemental carbon fraction in the smoke of at most 8%. Field burn experiments of logging residues gave values of the emission factor of elemental carbon

in the range of 0.08 to 0.12% Considering both laboratory and prescribed field burns, Patterson and McMahon (1985a,b) proposed an elemental carbon emission factor of 0.14%. In comparison, based on earlier compilations, the NRC and CGB studies adopted emission factors for elemental carbon of about 0.3 and 0.6%, respectively. In addition, the data of Patterson and McMahon (1985a,b) suggest that total smoke emission factors may also have to be reduced. Similarly, from a series of 35 measurements in 6 prescribed burns of forest products in the states of Washington and Oregon in the U.S., Hobbs et al. (1984) deduced an average smoke emission factor of only 0.4% for particles with diameters less than 2 μm.

Unfortunately, the results quoted above are all for small laboratory fires or for prescribed burns of logging residues, which are relatively low-intensity fires. Major forest fires may produce more smoke per mass of fuel and more intense fires are almost certain to produce more elemental carbon. Patterson and McMahon (1985a,b), in fact, show that the light absorption increases with fire intensity, indicating more elemental carbon emission. Clearly, field observations of these larger fires are urgently required. Also, Patterson and McMahon (1985a,b) mention that the burning of organic gases that are driven out of live vegetation might produce considerable soot. This could be an important source of elemental carbon in a nuclear war in which large amounts of live vegetation in forests and croplands are burned.

A large reduction in the estimates of the potential atmospheric optical impact from forest fires would follow from a study by Small and Bush (1985). Rather than assuming a wildland fire area proportional to total yield and global statistical coverage of forest, brush, grass, and agricultural lands, Small and Bush (1985) attempted to identify the exact locations of potential military targets (missile silos, air bases, radar sites, weapon storage depots, communication centers, etc.) and to calculate the ignition area, type of wildland and its fuel loading, firespread, and smoke production. The results of the calculation vary seasonally, but in all seasons Small and Bush (1985) found at least an order of magnitude less smoke production than estimated by Crutzen and Birks (1982), Turco et al. (1983a), CGB (1984), and NRC (1985).

Small and Bush (1985) point out that most military targets are not distributed randomly over the various ecosystems of the U.S. and U.S.S.R. but are either concentrated in a few missile fields, or located along major transportation arteries. According to their analysis, the greatest number of targets are located in agricultural and grasslands, while 14% are in forest lands, mostly in the Soviet Union. Burnable fuel loadings in each of the categories of wildlands and agricultural lands were taken from analyses of the U.S. Forest Service (Deeming et al., 1977). Small and Bush also assumed that croplands would not be in a condition to burn for most of the year, but only when grains have ripened and have not yet been harvested, a period of

about two weeks. Consequently, although only 10% of the military targets are located in forested lands, forest fires would still account for 40% of the total area burned.

Weather conditions could have a large influence on firespread, leading to substantial seasonal variations, with maxima during summer. In the study of Small and Bush (1985), average climatic conditions necessary for calculations of ignition radius (visibility and fuel moisture) and probability of firespread (temperature, relative humidity, fuel moisture, and winds) were obtained for weather stations closest to the potential targets. Altogether, Small and Bush (1985) derived a maximum forest fire area of 70,000 km^2 in summer time, about 30% of that adopted by the NRC and CGB studies, and total smoke emissions of at most 3×10^{12} g, an order of magnitude less than that derived in the earlier studies.

The study by Small and Bush (1985) currently is the most complete analysis of the possible wildland fire areas following a nuclear war. However, very little detail about their analysis procedures has been provided. Furthermore, there are critical factors and assumptions entering into their analysis that indicate that their estimates represent lower bounds to the smoke that would be produced from wildlands in a nuclear war.

First of all, the applicability of the adopted fire ignition and spread model, in which average meteorological conditions are assumed, is open to question. For instance, it is conceivable that large tracts of the Soviet Union are in a condition of drought, while those in the U.S. are not (and vice versa). The probability that major forest fires may spread over large areas of any one of the combatant nations due to regional drought conditions should be considered. It is exactly this factor that leads to large-scale forest fires during unfavorable years. For instance, there are reports of forest fires lasting for months and burning for some ten million hectare in Siberia (Shostakovitch, 1925). It is clear that firespread must have played a large role in this. The potential effects of fires started by tactical nuclear weapons (such as the 30,000 such weapons in the European theater alone) should also be taken into account.

In the study by Small and Bush (1985), firespread accounted for less than 7% of the total fire area. This is an extremely low number in light of the tabulated frequency distribution of fire danger indexes by Schroeder and Chandler (1966), partly reproduced in Table 3.6. According to this tabulation, in the period April–October, the probability of "critical fire conditions" in the Northern Plains regions would be between 3–23% and for "actionable conditions" near 50%. Critical conditions imply that any fire would be uncontrollable and could spread, until the weather changes. Actionable conditions imply that the fires can be controlled with fire fighting efforts. However, effective fire fighting would be very unlikely in a nuclear war situation.

TABLE 3.6.
EXPECTED FIRE BEHAVIOR (SCHROEDER AND CHANDLER 1966)

Fire condition[a]	January	April	July	October
Northeastern Plains Region				
FO	.93	.35	.23	.29
NS	.06	.22	.32	.25
Act	.01	.40	.43	.42
C	.00	.03	.02	.04
Northwestern Plains Region				
FO	.73	.34	.12	.22
NS	.15	.19	.13	.14
Act	.12	.41	.57	.50
C	.00	.06	.18	.14
Northern Rockies & Northern Intermountain Region				
FO	.90	.23	.03	.30
NS	.06	.31	.07	.20
Act	.04	.45	.72	.46
C	.00	.01	.18	.04
Central Intermountain Region				
FO	.72	.16	.02	.10
NS	.17	.15	.04	.11
Act	.11	.55	.43	.64
C	.00	.14	.51	.15

[a] The fire conditions considered are:

FO = Fire Out (fire won't start)
NS = No Spread (fire will start but won't spread and will go out if weather stays the same)
Act = Actionable (fire needs action and is controllable)
C = Critical (fire uncontrollable until weather changes)

Secondly, the fuel contained in the U.S. Forest Service Fire Danger Model, which was used by Small and Bush, accounts only for a small fraction of the potentially available fuels, i.e., only the "fast burning" fuels that mainly contribute to fire intensity. They suggest that the fires would consume 0.5–1.6 kg/m^2 in forests, which accounts for only 3–10% of the available biomass density. A range of 2–4 kg/m^2 seems much more realistic, especially since trees would be shattered by blast waves over wide areas.

Furthermore, it is a distinct possibility that the simultaneous ignition of forest and other wildland materials following nuclear attacks would become more efficient in a multiple burst scenario than under normal conditions because the overlapping blast wave and thermal radiation zones can shatter and dry out live and moist fuels, making them more susceptible to burning.

Finally, the analysis of fire ignition area and land use characterization derived by Small and Bush (1985) is not uncontested. A recent evaluation of land use in and around U.S. ICBM silo fields by Ackerman et al. (1985b) indicates that as much as 150,000 km^2 of vegetation could be affected in the summer half-year by attacks on U.S. silos alone, which should be contrasted with the 190,000 km^2 derived by Small and Bush (1985) for *all* military targeting. The difference in these estimates is partly related to the assumed incendiary efficiency of multiple nuclear bursts over missile fields.

The land use data derived by Ackerman et al. (1985b) from Landsat imagery and U.S. Geological Survey land use maps are reproduced in Table 3.7. Making use of a new survey of biomass loadings (see also Volume II of this report), these authors calculated the smoke emissions from forest and crop fires to be from 5 to 10 times greater than those derived by Small and Bush (1985). This difference is related to the larger area assumed affected as well as the larger estimates of readily combustible biomass. As a further complication, there are indications that more Soviet silo fields and military bases are located in forested areas than are U.S. bases.

TABLE 3.7.
LAND USE IN U.S. MISSILE BASES AS FRACTIONS OF THE TOTAL AREA (FROM ACKERMAN ET AL., 1985B)

Missile Base	Grass-lands	Deciduous Forest	Coniferous Forest	Agriculture	Other[a]
Ellsworth, SD	.74	—	.03	.22	.01
Grand Forks, ND	.03	.03	—	.94	—
Malmstrom, MT	.48	—	.12	.40	—
Minot, ND	.22	—	—	.73	.05
Warren, WY	.54	—	—	.45	.01
Whiteman, MO	—	.11	—	.87	.02

[a] Mainly water or barren land.

The estimations of the possible contributions of wildland fires to smoke production in a nuclear war remain, therefore, still uncertain. Following the studies of Hobbs et al. (1984), Patterson and McMahon (1985a,b), and Small and Bush (1985), it seems likely that their importance was somewhat overestimated in the previous studies. However, this does not significantly alter the total estimated emissions, which are dominated by the emissions from urban and industrial fires.

Finally, it should be noted that forest fires in the postwar environment might lead to important effects. It is conceivable that large quantities of unburned and dead forest material could accumulate due to the combined effects of climate changes and the release of intense radioactivity (Woodwell,

1982) and hazardous chemicals from industrial and urban targeting. If ignited some months after the nuclear war, these areas could contribute large amounts of smoke, although by this time it may not be a significant contributor to climatic effects. Peatbog fires in north temperate latitudes, which can last for months (Shostakovitch, 1925; Safronov and Vakurov, 1981) are another potential source of large amounts of smoke.

3.5 MICROPHYSICAL PROCESSES

In the preceding sections, estimates of smoke emission from fires were given. The particles or aerosols, comprising this smoke (and the dust raised by surface bursts—see section 3.8) interact with each other and with background particles, clouds, and precipitation as they evolve in the atmosphere. Accordingly, a variety of physical processes involving heterogeneous mixtures of airborne particles are of interest here. The properties that define a particle include its size, shape, structure (morphology), composition, density or mass, index of refraction, and response to humidity. These properties can also change in time through the physical and chemical transformations outlined below.

3.5.1 Interactions With the Environment

Smoke and other aerosols in the atmosphere are influenced by gravity and interact with ions, gases, solar radiation, and, near the ground, physical surfaces. Gravitational sedimentation occurs when a particle falls relative to the surrounding air because of its much higher density (compactness). Sedimentation may generally be neglected for submicron particles in the troposphere and lower stratosphere (Twomey, 1977) because vertical atmospheric motions transport such particles more rapidly than sedimentation. For larger particles, however, sedimentation enhances the rate of removal by bringing particles to lower altitudes or to the surface. An exception would be loosely aggregated clusters (e.g., soot-like chains), with very low effective densities and large effective aerodynamic cross-sections. Such particles would readily be carried by winds, and would settle out of the atmosphere more slowly than compact particles of the same mass.

Near the ground, particles can diffuse (and adhere) to a variety of surfaces, including soil, water, and vegetation (the latter in particular may provide an enormous collection area in heavy overgrowth). Particles of different sizes attach to surfaces with different efficiencies. Notably, aerosols with radii in the range of 0.1 to 1.0 microns have very small "deposition" velocities (less than 0.001 m/sec; Slinn, 1977). The deposition velocity is defined in terms of the net flux of a substance carried to a surface by all active microscale processes. Nevertheless, for smoke particles in the submicron size range, dry deposition can be an important secondary removal process.

Aerosols exist in close thermal equilibrium with the atmosphere. The temperature deviation is usually negligible because the energy absorbed by small particles (e.g., solar radiation) is quickly transferred to the surrounding air by thermal diffusion. Hence, nonequilibrium heating or cooling of smoke particles or fine dust particles may be ignored in the lower atmosphere. Above the middle stratosphere (roughly 35 km), particles may heat up by several degrees above the surrounding air temperature.

Smoke interacts with gaseous chemical constituents in the atmosphere. Some of the reactions alter the surface composition of the particles, while others may actually consume the smoke. Adsorption of vapors from the environment can also change the composition and size of particles as well as their hygroscopic properties and index of refraction. The reactions of oxidants such as ozone and hydroxyl radicals with carbonaceous soot particles may deplete the soot mass; such reactions could be particularly important in the stratosphere where a long residence time for soot would otherwise be expected. However, reactions that are sufficiently rapid to merit attention in the atmosphere have not been identified (see Chapter 6). Therefore, significant soot consumption by photochemical processes must be considered speculative at this time. Moreover, particles would be coated by oily material or, after a day or so in the atmosphere, with a number of inorganic compounds such as sulfates and water, thereby isolating the carbon surfaces from direct chemical attack.

Ions are present at all levels in the atmosphere. In the troposphere, ion concentrations of $10^9/m^3$ are typical. Because the mobilities of positive and negative ionic species are generally unequal, aerosols immersed in an ion plasma accumulate a net charge. The charge is small enough that its effects on aerosol microphysical processes can usually be ignored (Twomey, 1977). This situation is quite different from that which applies in powerful convective storm systems (and possibly large fire plumes), where ice processes lead to strong electrification of cloud droplets and aerosols (Pruppacher and Klett, 1980). Because air is a weakly ionized plasma with a small but finite conductivity, any highly charged objects immersed in it will tend to discharge over time.

Photophoresis describes the force exerted on a particle as a result of nonuniform heating by solar (or other) radiation. If, in absorbing an incident beam of radiation, a particle is heated preferentially on one side, the diffusion of heat away from the particle creates a thermal gradient in the surrounding air which exerts pressure in the opposite direction. By its nature, the photophoretic force is very weak. However, for small particles illuminated by sunlight, it can exceed the force of gravity. Recently, Sitarski and Kerker (1984) proposed that photophoresis may cause soot particles to levitate in daylight, and might explain the long lifetime of the Arctic haze aerosol. Depending on the size and composition of the particles,

photophoresis could either increase or decrease the vertical (settling) velocities of soot aerosols. However, there are a number of reasons to believe that photophoresis is unlikely to be important for soot under atmospheric conditions: Brownian rotation of small particles reduces their nonuniform heating by sunlight; the diurnal variation of solar insolation reduces the average photophoretic force by a factor of about four relative to the gravitational force; the irregular shape of typical soot particles disturbs the required pattern of heating; upwelling shortwave radiation (scattered and reflected) heats the particles in the opposite sense from the direct solar radiation; and the solar beam could be significantly attenuated in certain circumstances following a nuclear war.

3.5.2 Agglomeration

A homogeneous or heterogeneous aerosol mixture will coagulate through various mechanisms to form aggregated particles. Collisions between particles are induced by thermal Brownian motions, winds and turbulence, and gravitational settling. Coagulation due to Brownian motion is most effective for submicron particles and is generally less significant for supermicron particles (Pruppacher and Klett, 1980). Collisions between particles traveling at different relative speeds in laminar flows and in turbulent flows are most important for larger particles, which can experience differential accelerations due to wind shears, and can cross streamlines during curvilinear acceleration. Gravitational coalescence involves differences in particle fallspeeds, in which a larger particle overtakes and intercepts a smaller particle. To be effective, the fallspeeds must be substantial; accordingly, at least one large particle must be involved in the collision process. The relative importance of the various aerosol agglomeration mechanisms is illustrated in Figure 3.1.

If an encounter between two particles is to result in coagulation, the particles must touch and adhere. Submicron particles with small Stokes numbers tend to flow around obstructions in the airstream. To impact a surface, such particles must diffuse through a laminar boundary layer separating the surface from the deflected airflow. However, because aerosols have (relatively) small diffusion coefficients, they are hindered in reaching the surface during the brief duration of an encounter. Larger particles with greater inertia can cross streamlines in the flow and impact the surface directly.

A variety of forces can act to hold the aerosols together following a collision. Van der Waal's surface forces can hold dry, submicron aerosols together. Droplets can coalesce into larger droplets under the influence of surface tension, and dry particles can be wetted in this manner. For large dry aerosols, electrical coulombic forces can effectively bond particle clusters, given a sufficient charge. Chemical substances condensed on surfaces and in crevices can act to cement and strengthen particle aggregates.

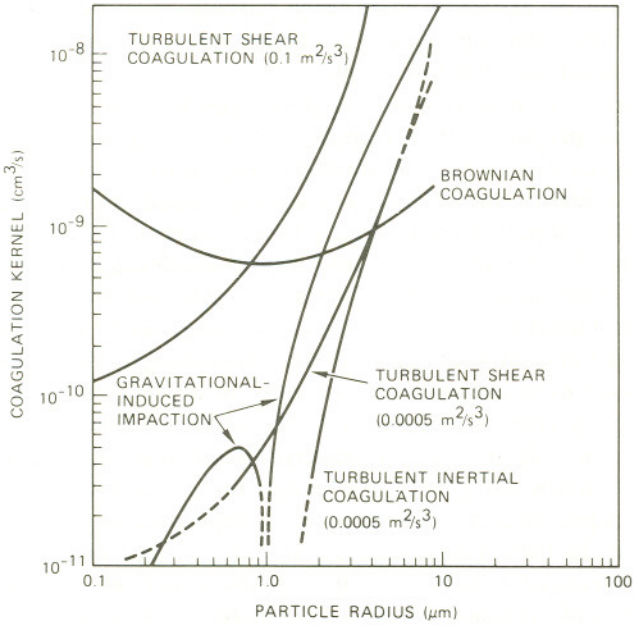

Figure 3.1. Comparison of coagulation kernels for various aerosol collision mechanisms for a spherical particle having a radius of 1 μm and a density of 1 g/cm^3 interacting with spherical particles having radii between 0.1 and 10 μm. The dotted lines indicate regions where complex hydrodynamic interactions between the particles invalidate the theoretical treatment used. The assumed turbulent energy dissipation rates are given in brackets. (Hidy, 1973, adopted from Pruppacher and Klett, 1980)

However, when particles impact with great force, they may not stick together. The particles can rebound elastically or, if there is enough force, can break off or knock loose smaller particles (Rosinski and Langer, 1974).

As already noted, large soot aggregates have been observed in the burning of oil and plastics (e.g., Day et al., 1979). In regions of flames that are hot, rich in organic molecules, and lacking oxygen, soot is initially generated as a concentrated aerosol of very small amorphous carbon spheroids roughly 50 nm in diameter (Wagner, 1980). The spheroids, which appear to be charged, coagulate to form chain structures, and the chains may later coagulate to form fluffy aggregates. If the sooty smoke is rapidly diluted, the chains are "frozen out" at fairly small sizes (less than 1 μm). If the smoke is very dense, the chains can aggregate to much larger sizes (greater than 10 μm). The rate of dilution of the smoke with clear air is an important factor in controlling the aggregate sizes (NRC, 1985). Typical dilution rates normally limit the extent of aggregation to relatively small sizes. Nevertheless, in large oil fires, where soot yields might exceed 10%, many supermicron agglomerated

particles would be expected. Such large particles may be efficiently scavenged by falling raindrops. These problems have not yet been quantified either experimentally or theoretically.

It is important to note that soot agglomerates have very different physical and optical properties than compact spheres of equivalent mass. Physically, soot agglomerates have abnormally large aerodynamic cross sections for their mass. Hence, they have lower settling velocities and smaller impact efficiencies than is suggested by their physical dimensions. The exaggerated cross sections of soot particles can also lead to accelerated coagulation rates (Baum and Mulholland, 1984). Instruments designed to measure aerosol sizes by optical means or by mobility analysis have, to our knowledge, never been calibrated against soot agglomerates. Accordingly, in situations where soot clusters are expected to form, such measurements must remain suspect. The optical properties of soot are discussed in the section 3.6.

In the plumes of large fires, the powerful winds that are induced loft ash, dust, and fire debris along with smoke and soot. Sub-micron smoke particles may be captured and removed by large supermicron particles that may also be lofted. In their global scale calculations, Turco et al (1983a, b) included the effects of modest quantities of fire-generated ash particles and large quantities of explosion-generated dust particles as scavengers of smoke. The collection processes that they treated included Brownian coagulation, gravitationally-induced impaction, and turbulent shear, and inertial coagulation (Pruppacher and Klett, 1980). For assumptions of both instantaneous and delayed dispersal of the mixed smoke and dust clouds, Turco et al. found these processes to be of minor importance.

Porch et al. (1985) have further examined the potential for scavenging by large particles, especially in firestorm environments. They considered turbulent energy dissipation rates ranging from 0.1 m^2/sec^3 typical of thunderstorms to 0.8 m^2/sec^3 scaled from the values for an intense fire plume modeled by Cotton (1985). The Porch et al model included a simplified turbulent coagulation theory, but did not account for the hydrodynamic interactions between large and small particles which generally reduce particle collection efficiencies (Pruppacher and Klett, 1980). They also did not include, however, the extra surface area of chained aggregates and the effects of particle charge, which may increase collection efficiencies. For levels of large particle concentrations ($\sim$ 0.1 g/m^3) found in a modest-sized fire by Radke et al (1983), there is very little reduction of the optical depth over a thirty minute period, which may actually be longer than typical smoke parcels would remain in the highly turbulent regions of the fire plume. In their model, large particle concentrations must be increased by about a factor of 50 (i.e., to levels observed near the ground in modest-sized dust storms) for there to be a reduction by a factor of 2 in optical depth. Maintenance of such high concentrations of large particles would require relatively high

windspeeds to scour the surface and loft dust, char, and other materials. Such conditions might occur as a result of the high velocity rotating winds induced in an organized urban firestorm (e.g., as may have occurred in Hamburg). If such events are as relatively rare as was the case during World War II, the overall effect on the total smoke burden as a result of scavenging by large particles would not be substantial; if such events are frequent, further consideration of this process may be warranted.

3.5.3 Precipitation Scavenging

The primary means by which submicron aerosols are removed from the atmosphere is through incorporation of aerosols into cloud water by nucleation and phoretic scavenging, followed by cloud water coalescence and precipitation to the ground. These same processes would be the primary removal mechanisms following a nuclear war. However, in discussing scavenging and aerosol removal, the prompt scavenging of smoke and dust by precipitation that may be induced in the convective fire plumes must be distinguished from the synoptic scale scavenging processes, which would occur after the smoke plumes had dispersed into the background atmosphere.

3.5.3.1 Observations

One of the most critical problems in the estimation of the long term climatic effects of large urban fires is the extent to which smoke particles could be removed by precipitation scavenging in the convective plumes that accompany the fires. The "black rains" that followed the nuclear explosions in Hiroshima and Nagasaki amply demonstrated that smoke can be removed from plumes by fire-induced convective clouds. A graphic illustration of this process can be seen in the Peace Memorial Museum at Hiroshima, where a section of the white wall of a house covered with streamers of ink-like smoke residues is displayed (Ishikawa and Swain, 1981).

Nevertheless, quantitative information on the efficiency of smoke removal by fire-induced precipitation is lacking. The efficiency is unlikely to be close to 100%. For most convective storm systems, the precipitation efficiency, which is roughly defined as the ratio of the precipitation rate at the ground to the water condensation rate in the cloud, is typically between 15% and 65% (Foote and Fankhauser, 1973; Marwitz, 1974; Hobbs and Matejka, 1980). Strong updrafts carry some of the condensed water to high altitudes, where it detrains from the clouds and reevaporates. Much of the rainfall below the cloud-base is known to evaporate as well (amounting to about 40% of the vapor flux into the cloud-base); however, this would have a lesser effect on the re-injecton of aerosols since few droplets evaporate completely. Overall, continental cumulonimbus systems typically convert less than 50%

of the moisture entrained into precipitation at the ground. In the case of very powerful cumulonimbus systems in highly sheared environments, the precipitation efficiency can be less than 15% (Fritsch and Chappell 1980). For one thing, the strong updrafts restrict the formation of large ice particles. Because precipitation is less efficient in this case, larger quantities of ice are injected into the anvil.

The ratio of condensible water mass to smoke mass in a large fire plume in a moist ambient environment could be 1000 or more (NRC, 1985). Accordingly, there is sufficient water available to remove most of the smoke—if the cloud were to rain and if the rain were efficient at scavenging the smoke. As just noted, intense cumulonimbus systems are generally inefficient generators of precipitation. Even so, enough rain/hail could form (in humid environments) to remove a significant fraction of the smoke.

Fires do not always produce intense convective plumes, rainfall, and efficient smoke scavenging. This is clearly illustrated by observations of major forest fires. In September 1950, the smoke plumes from more than 100 forest fires in Alberta, Canada resulted in the "Great Smoke Pall" over North America. Sunlight was attenuated over much of Canada and the eastern one-third of the U.S. (Wexler, 1950). The reported altitude of the smoke cloud was between 2.5 and 4.5 km. One week later, the smoke clouds were visible over several countries in Western Europe, where the smoke was observed to be as high as the tropopause (Smith, 1950; Wexler, 1950).Satellite observations show that smoke produced by large forest fires in European Russia in August 1972 was transported eastward over the Ural mountains for distances of 5600 km in the middle troposphere (Grigoriev and Lipatov, 1978). Similar observations of long range transport of Australian forest fire smoke to New Zealand are common (D. Lowe, private communication). Such evidence indicates that the smoke produced by forest fires generally escapes prompt precipitation scavenging and disperses through the atmosphere.

In general, large oil fires appear to produce soot plumes in which little condensation or precipitation due to fire-induced convection occurs (Davies, 1959). Such plumes typically rise to several kilometers altitude. Radke et al. (1980a) observed soot coagulation in the plume of the Meteotron (a soot-generating oil-fired 1000 megawatt artificial heat source in France). They also noted that the smoke was capable of dissipating ambient clouds above the Meteotron. Following dozens of tests, precipitation associated with the operation of the Meteotron was observed only once (in an unstable air mass).

Radke and coworkers (Radke, private communication) observed smoke "processing" by a condensation cloud over a prescribed forest fire in 1978 (processing refers to the scavenging of smoke particles by water droplets, with re-emission through cloud evaporation). They measured the size

distribution and visible backscatter coefficient of the smoke in two air parcels in the plume; one parcel passed through the capping condensation cloud, and one passed beneath (and clear of) the capping cloud. The cloud-processed smoke had considerably fewer particles of very small size (a factor of about 10 less at sizes less than 0.05 μm radius), had a somewhat larger number of particles in the intermediate size range (approximately 0.1 to 1.0 μm), and had fewer particles in the supermicron size range. The scattering coefficients for the two smoke samples were about equal (absorption was not measured), possibly suggesting only limited impact of processing on the overall optical properties of the smoke. However, the experiment involved a relatively small cloud formation, and was not strictly controlled (i.e., by sampling in the same smoke parcel before and after the cloud). Accordingly, the results are only suggestive of potential effects.

3.5.3.2 Nucleation

Nucleation occurs when water vapor in excess of the saturation vapor pressure condenses onto aerosol surfaces, forming water droplets or ice crystals. For ambient hygroscopic aerosols, nucleation in clouds is probably the dominant scavenging and removal mechanism (Pruppacher and Klett, 1980; Twomey, 1977). On the other hand, experimental evidence from fire plumes suggests that smoke, particularly sooty smoke, is less susceptible to nucleation scavenging.

In typical convective clouds, water vapor supersaturations seldom exceed 1%, because of the abundance of nuclei and particle surfaces to absorb the excess moisture (Pruppacher and Klett, 1980). However, the larger the convective velocity, the greater the supersaturation that could theoretically be achieved. In a fire column, high vertical velocities would be associated with enhanced concentrations of windblown debris such as ash, char and dust. Accordingly, the enhanced surface area for condensation may limit the supersaturation to normal values. Cloud condensation nuclei (CCN) are defined as those particles that can be nucleated into water droplets at supersaturations of a few percent or less.

Forest fires are potentially major sources of cloud condensation nuclei. Eagan et al. (1974) observed the production of as many as 6×10^{10} CCN active at 0.5% supersaturation for each gram of forest fuel consumed. The CCN activity may be due to the chemical nature of the smoke particles, which have been determined to consist of complex organic compounds with little amorphous carbon, or soot. Bigg (1985) reported other measurements in forest fire plumes in which about 5% of the total number of particles were active as CCN at 1% supersaturation, and 0.5% at 0.25% supersaturation. Moreover, the proportion of CCN did not appear to increase as the smoke aged. The data of Eagan et al. (1974) and Bigg (1985) are generally consistent

if a smoke emission factor of about 1% and a mean particle size of 0.1 μm—values commensurate with observations—are assumed.

If a production rate of 6×10^{10} CCN/g is assumed for the burning of cellulosic materials in urban centers, a total of 1 to 4×10^{26} CCN active at 0.5% supersaturation could be produced in the nuclear war scenarios of NRC (1985) and Crutzen et al. (1984). This is of the same order of magnitude as the total global abundance of background CCN (Pruppacher and Klett, 1980).

Soot particles tend to be hydrophobic (i.e., water repellent), particularly fresh soot that has not had a chance to collect hygroscopic compounds. For the atmospheric conditions that prevail in Western Europe, observations by Ogren and Charlson (1984) show that soot particles are removed at a slower rate than sulfate aerosol for the first few days following emission. Radke et al. (1980a) measured CCN abundances in the large sooty plume generated by the Meteotron device. They found concentrations very close to background levels (approximately 500 to 1200/cm^3 for supersaturations of 0.5 to 1%, respectively). At the same time, the total smoke particle concentrations exceeded 10^4/cm^3, suggesting that only a small percentage of the soot particles were active as CCN. Similarly, in carefully designed laboratory experiments currently underway, Hallett and coworkers (personal communication) have noted that some fresh and aged soot particles can be active as CCN at approximately 1% supersaturation; these CCN typically comprise a small percentage of total soot particle population.

Little information is available on the ice-nucleating properties of smoke and soot. Such particles should be poor ice nuclei (Pruppacher and Klett, 1980). Bigg (1985) reports that sampling in forest fire convective columns yields ice nuclei concentrations of approximately 0.01/cm^3 (while this is roughly 100 times greater than ambient ice nuclei concentrations, it is obviously much smaller than the total smoke particle concentration). A substantial increase in ice nuclei abundances could affect the microphysical development of fire-induced clouds, and should be considered in future studies.

Several factors could enhance smoke nucleation rates in fire plumes. Large aggregated smoke or soot particles might nucleate more readily than the smaller particles sampled in the experiments cited above. Chemical transformation of smoke particles—e.g., coating by sulfates generated from sulfur in the fire fuels—make the particles more susceptible to water condensation. Turbulence in the plume could also create local zones of considerably higher supersaturation.

On the other hand, in the larger fire plumes, characterized by intense convection, the time available for agglomeration and chemical transformation prior to condensation is only a minute or so, which seems insufficient for major physical or chemical changes to occur. Moreover, as already noted,

the supersaturations in the plume are likely to be suppressed by the presence of windblown fire debris particles.

If most of the smoke particles in the plume were to nucleate, and the particle concentrations were as high as 10^4 to $10^5/cm^3$, the clouds formed could become overseeded, i.e., composed of a large number of very small droplets. Such clouds are less likely to produce precipitation because droplet coalescence is less efficient (Twomey, 1977). However, ultragiant nuclei raised by fire winds would continue to provide a source of precipitation-sized water particles. As these fell through the cloud, smaller smoke and dust particles could be scavenged and washed out (Hobbs et al., 1984). The most efficient removal would occur if the smoke particles had absorbed water and reached a size of several microns radius. These expanded smoke particles could then be collected relatively efficiently by inertial impaction on the precipitation drops nucleated on ultragiant aerosols, provided that an adequate supply of these latter particles existed.

Because observational data suggest that only a small fraction of all the smoke particles would be active as CCN, most of the smoke would have to be scavenged by processes other than nucleation. These are discussed below.

3.5.3.3 Brownian, Inertial and Phoretic Scavenging

For smoke particles with a radius on the order of 0.1 μm, Brownian and inertial collection by cloud and precipitation drops can generally be ignored (Pruppacher and Klett, 1980). For aerosols with radii much less than 0.1 μm, Brownian diffusion is important, while for aerosols with radii much greater than 0.1 μm, inertial impaction is important (particularly for those particles with radii greater than several microns). The limited fire plume and microphysics modeling accomplished to date also indicates that phoretic scavenging processes are dominant over Brownian and inertial processes (Cotton, 1985; see also Chapter 4).

Phoretic scavenging occurs when aerosols, primarily in the submicron size range, are brought into contact with a water droplet or ice crystal through motions induced by fluxes of heat and mass. Thermophoresis represents aerosol motion induced by the flux of heat to an evaporating droplet or ice crystal. As the droplet evaporates, heat is absorbed from the immediate vicinity of the droplet, producing a local thermal gradient. The corresponding gradient in the kinetic energy of air molecules then drives the aerosol in the direction of the heat flux (Pruppacher and Klett, 1980). At the same time, an outward diffusive flux of water molecules is associated with an evaporating droplet. This flux establishes a weak hydrodynamic Stephan flow of air away from the droplet. Collisions between the aerosol and the flowing air molecules cause the particles to drift away from the evaporating droplet. The resulting diffusiophoretic force opposes, but is generally

less than, the thermophoretic force. As a result, evaporating droplets or ice crystals are effective in collecting aerosols; likewise, growing droplets tend to repel aerosols by this mechanism. Phoretic scavenging is generally much weaker for ice crystals than water droplets because the evaporation rates of ice crystals in clouds are normally much lower (although the time scales can be longer, particularly in the cloud anvil).

The relative importance of Brownian diffusion, inertial impaction and phoretic forces in the scavenging of an aerosol by precipitation, based on theoretical calculations, is illustrated in Figure 3.2 (Slinn and Hales, 1971). Of particular interest is the regime corresponding to aerosol radii of 0.1 to 1.0 μm where all scavenging mechanisms are relatively inefficient. Within this region, known as the Greenfield gap (after Greenfield, 1957), phoretic effects are the most important (NRC, 1985).

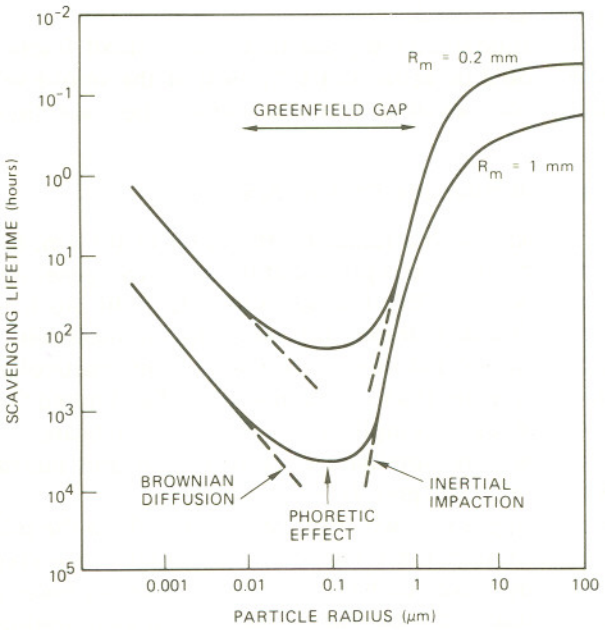

Figure 3.2. Calculated e-folding lifetimes of aerosols against removal by precipitation of 10 mm/hr, for precipitation drop spectrums with characteristic drop radii of R_m = 0.2 and 1.0 mm. The dominant scavenging mechanism in each aerosol size range is indicated (from Slinn and Hales, 1971, reproduced by permission of American Meteorological Society)

It should be noted that there is still disagreement over the magnitude of phoretic scavenging rates in clouds, and indeed over the sign of the net force (thermophoretic minus diffusiophoretic) (Vittori, 1984). It also has been suggested that other forces (e.g., electrical) may act to fill the

Greenfield gap, thereby reducing the atmospheric lifetime of sub-micron particles. Current experimental evidence bearing on this issue is mixed. Accordingly, theoretical calculations of aerosol scavenging rates should be treated as tentative estimates at this time.

3.5.3.4 Smoke Aging

Smoke particles and chemical vapors scavenged by cloud drops and ice crystals that later evaporate above or below the fire plume are released as an "aged" smoke. Particles that are not subject to water condensation can also age by coagulation with other smoke particles, agglomeration with fire debris and ambient aerosols, and deposition of chemical vapors. Particles that are aged for several days in the background atmosphere, and those passing through cloud condensation/evaporation cycles are expected to be fairly compact and hygroscopic in nature. Large soot agglomerations, for example, might collapse under surface tension if wetted, and thus could become denser and more spherical.

As mentioned earlier, the process of aging by water condensation has been observed in a forest fire plume (Radke, private communication), and aging by coagulation, in an oil fire plume (Radke et al., 1980a). Nevertheless, except for the general facts already described, extensive data on smoke aging in various atmospheric environments are not available.

3.5.3.5 Overall Scavenging Efficiency

Theoretical models of precipitation scavenging generally underestimate the aerosol removal rates actually observed in clouds (e.g., Radke et al., 1980b). There are several apparent reasons for this discrepancy. The theoretical models are not yet sophisticated enough to account for all of the possible simultaneous interactions of aerosols with water droplets and ice crystals, including the effects of electrical charge, turbulence, and transient phenomena. The physical properties of the aerosols are also important. Radke et al. (1980b) attributed the larger than predicted precipitation scavenging efficiencies of aerosols from power plant plumes to the hygroscopic nature of the particles, which they proposed could swell in size by absorption of water vapor, thereby filling the Greenfield gap. Prodi (1983) observed that ice crystals growing in the presence of supercooled water droplets readily collected submicron hygroscopic salt aerosols, but not submicron hydrophobic wax particles. Most atmospheric scavenging observations involve aerosols that are readily nucleated in clouds, or on which water readily condenses. Smoke, on the other hand, has different physical characteristics and, one might expect, lower scavenging and washout efficiencies.

An hour or less of steady rainfall (of up to 10 mm of water) is generally

capable of removing most aerosol pollutants from the atmosphere (Pruppacher and Klett, 1980). The induced precipitation in a fire plume would (for a particular air parcel) probably be much shorter in duration, but more intense.

Because the prompt scavenging of soot particles in fire-induced convective columns depends on many factors that are poorly known and extremely difficult to predict, the overall scavenging efficiency can only be crudely estimated. Clearly, a much better understanding of individual scavenging processes is required in order to make a reliable estimate. In previous studies, assumptions of 30 to 50% prompt removal of smoke (from fire plumes) have been made (Turco et al., 1983a,b; NRC, 1985; CGB, 1984). These values seem to be reasonable given the current state of knowledge (Hobbs et al., 1984).

In determining the synoptic-scale scavenging of smoke from the background atmosphere, three factors play an important role: the injection height of the smoke, the composition and morphology of the smoke particles that survive prompt scavenging, and the possible large-scale meteorological perturbations of the atmosphere. One plausible approach is to assume that the smoke particles, once processed through a condensation cloud over a large fire or a natural cloud system, can be efficiently removed during subsequent encounters with clouds and precipitation in synoptic systems. Thus, Malone et al. (1985), in their climate study using a general circulation model, assumed that smoke was essentially completely removed whenever entrained into a precipitating cloud system. This may in fact overestimate the removal rate because, in such models, precipitation occurs simultaneously over an entire grid cell, which is typically on the order of 10^5 km^2, whereas precipitating clouds are generally confined to only a fraction of this area (see Chapters 4 and 5).

While the physical characteristics of the smoke particles that escape the fire plumes have not been determined, they would presumably vary widely. Some particles would be in a relatively unaltered state, while others would be well "aged". Hence, the initial efficiency for subsequent scavenging by mesoscale and synoptic scale cloud systems could also vary widely.

3.5.4 Smoke Lifetimes

The residence times of atmospheric aerosols depend on their chemical composition, morphology and sizes. Soot generated from oil combustion is generally hydrophobic and resistant to water nucleation (Radke et al., 1980a). However, if the soot coagulates into larger particles, it may interact more strongly with water (Bigg, 1985). The smoke produced in urban and industrial fires would be coated with hygroscopic materials as it aged, making it more susceptible to removal by clouds and precipitation.

Under normal atmospheric conditions, the e-folding lifetime of atmospheric aerosols with radii less than 0.1 μm is shorter than a few days (Jaenicke, 1981). Particles with radii larger than a few microns are likewise removed rather rapidly from the ambient troposphere by precipitation scavenging and gravitational settling (although fluffy aggregates would settle out much more slowly). Aerosols with radii between about 0.1 and 1.0 μm have the longest lifetimes, generally on the order of a few days to a week in the lower troposphere, a month in the upper troposphere, and 1–2 years in the lower stratosphere (Jaenicke, 1981). Particles in this Greenfield gap size range also happen to affect sunlight most effectively (see the following section and Chapter 4).

It is important to remember that, if atmospheric stability and precipitation rates were greatly perturbed following a nuclear war, aerosol removal rates and lifetimes would be altered accordingly. In particular, if increased stability and reduced precipitation occurred on a hemispheric scale, as now seems likely (see Chapter 5), the atmospheric lifetime of smoke could be lengthened considerably. The stabilization process involves the absorption of solar radiation by smoke, which is described in the next section.

3.6 OPTICAL PROPERTIES

The primary means by which the smoke and dust injected into the atmosphere by nuclear explosions and fires affects atmospheric processes is through interaction with solar and thermal radiation. Thus, the determination of the optical properties of the aerosol is a critical factor in assessing the climatic impact. The optical properties are functions of the composition of the aerosol, of the morphology (shape) of individual particles and of the size distribution of the aerosol. As noted in the preceding sections, the composition of the smoke is determined by a complex interaction of fire intensity, fuel type and loading, particulate emission factors, and fire duration. Particle morphology and size distributions are determined by formation processes and subsequent microphysical processes. Because the physical properties of the particles are changing with time, the optical properties are also subject to change with time.

Given the complexity of the particles, it is not possible to derive exact expressions for their optical properties. Measurements of the optical properties of smoke from large fires are extremely limited. In order to arrive at an estimate for the optical properties, two approaches will be followed. First, the optical properties of idealized spherical particles will be discussed and then applied to smoke. Secondly, a simple extrapolation of laboratory measurements of the properties of elemental carbon will be carried out to infer the optical properties of smoke. Finally, some observations that bear on the problem will be considered.

3.6.1 Optical Coefficients

The optical coefficients of atmospheric particles are usually computed using Mie theory for homogeneous (i.e., uniform composition) spheres. Rigorous theoretical models are also available for some symmetric shapes such as spheroids (Asano and Sato, 1980). In order to carry out these calculations, the size of the sphere and the index of refraction of the material of which it is made must be known. The index of refraction is a physical property of the material related to its ability to reflect and absorb electro-magnetic radiation and can be measured by a variety of techniques. In addition to the exact theories, some approximate theories have been developed for irregularly shaped particles (Pollack and Cuzzi, 1980).

For homogeneous spheres, a convenient quantity used to describe the interaction between aerosol particles and electromagnetic radiation is the Mie size parameter x, defined as

$$x = \frac{2\pi r}{\lambda} \tag{3.1}$$

where r is the particle radius and λ is the wavelength of the radiation. The particle-field interaction is often expressed in terms of the extinction efficiency, Q_e, which is defined as the ratio of the cross-section for extinction (i.e., the effective total cross-section of the particle as seen by the electromagnetic radiation) to the geometric cross-section. For a given material and, hence, a known index of refraction, Q_e is only a function of x. Typically, the particle-field interaction (and Q_e) has a maximum value when x is of order 1. For large x, Q_e tends asymptotically to a value of 2 due to diffraction effects; for small x and no absorption, Q_e decreases rapidly as x^{-4} (the Rayleigh regime). Thus, the interaction is greatest when the particle size and the photon wavelength of the electromagnetic radiation are comparable in size. Intuitively, this means that the maximum effect per unit mass of material on a radiation field is achieved by subdividing that material into particles with diameters approximately equal to the photon wavelength. Particles much smaller than the photon wavelength have only a minimal effect on the photon.

The extinction efficiency of a particle Q_e is the sum of its scattering efficiency, Q_s, and its absorption efficiency, Q_a. Radiation which is scattered by the particle is simply re-directed from its original direction of propagation to some other direction (although the majority of the scattered radiation continues on in nearly the same direction of propagation). Radiation which is absorbed by the particle, on the other hand, is removed from the propagating beam and converted to some other form of energy, usually heat. Obviously, for nonabsorbing particles, $Q_s = Q_e$. For absorbing particles, the partitioning between scattering and absorption depends on the index

of refraction (i.e., the material of which the particle is composed) and the size parameter. At small values of x, absorption dominates scattering and $Q_a \sim Q_e$. At large values of x and for strongly-absorbing material, Q_a and Q_s are roughly equal. (Detailed treatments of Mie theory and efficiency factors are available in a number of texts such as Kerker, 1969 or van de Hulst, 1957).

Solar energy is emitted predominantly at wavelengths between 0.3 and 2 μm, with a maximum at about 0.55 μm. Wavelengths of the thermal infrared radiation produced by bodies with temperatures around 0°C or 273 K are in the range of 5 to 50 μm. The representative wavelength for the thermal infrared radiation is usually chosen to be 10 μm, both because peak emission occurs at about this wavelength and because the Earth's atmosphere is essentially transparent to radiation at this wavelength, which means maximum cooling of the Earth's surface occurs due to radiation in this spectral region. (see Chapter 4 for a more extended treatment of the radiation budget of the Earth and atmosphere). Thus, the ratio of the wavelength of maximum thermal emission (10 μm) to the wavelength of maximum solar energy is about 20. For a material with approximately equal values of refractive index both wavelengths, solid spheres with radii less than 0.5 μm absorb about 20 times more energy at visible solar wavelengths than at thermal infrared wavelengths, and are on the order of 10^4 times more efficient at scattering visible light than thermal infrared radiation. Since a typical distribution of atmospheric aerosols produced by combustion processes has a mean, or average, particle radius on the order of a few tenths of a μm, the distribution typically has a maximum extinction efficiency at wavelengths on the order of 0.5 to 0.6 μm, which coincides with the maximum energy emission of solar radiation. At a wavelength of 10 μm, $x \sim 0.05$ and the value of Q_e is substantially less than at a wavelength of 0.5 μm.

Several cautionary notes should be added to the discussion in the preceding paragraph. First of all, because atmospheric aerosols exist in a range of particle sizes, the extinction efficiency for the distribution at a particular wavelength is a weighted average of the efficiencies of the individual particles at that same wavelength. In general, this averaging tends to reduce the variation in the values of the efficiency factors with wavelength. Secondly, many materials have larger indices of refraction (and, hence, larger extinction efficiencies for a given value of x) at thermal infrared wavelengths than at visible wavelengths. This also tends to increase the value of Q_e at thermal wavelengths relative to visible wavelengths. As a rough rule, Q_e for atmospheric aerosols at 10 μm is about 1/10 the value of Q_e at 0.5 μm.

To illustrate these points, values of Q_e and Q_a have been computed from Mie theory for spheres as a function of wavelength from 0.2 to 30 μm (Figure 3.3). The spheres are assumed to have a complex index of refraction of 1.55–0.1i at all visible wavelengths, as suggested in the NRC report (1985).

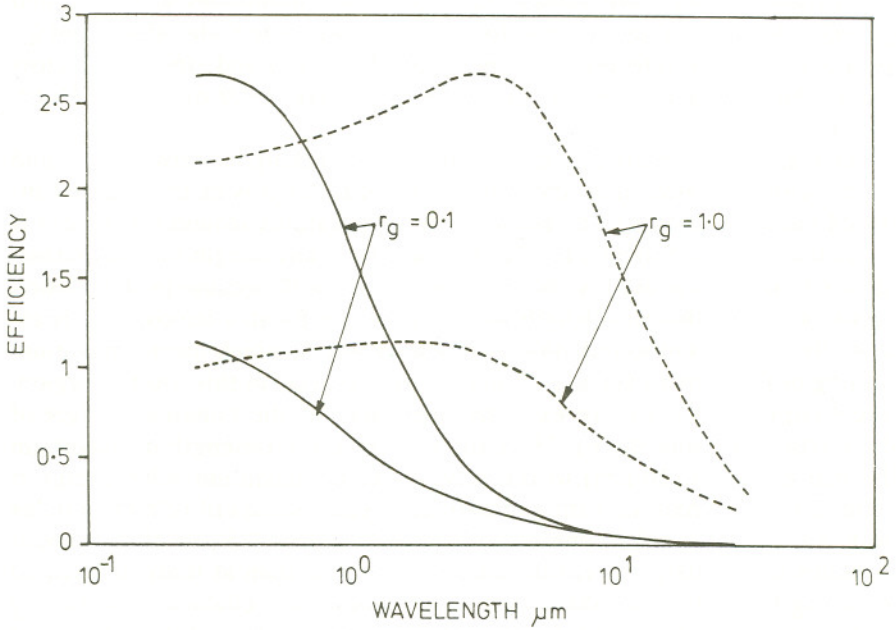

Figure 3.3. Extinction efficiency (upper curve) and absorption efficiency (lower curve) as a function of wavelength for absorbing aerosols (index of refraction = 1.55 − 0.1i). Solid curves are for a size distribution with a number mean radius, r_g, of 0.1 μm, dashed curves for a number mean radius of 1.0 μm

While there are some indications that the imaginary part of the refractive index, and thus the absorption efficiency, of sooty material may increase somewhat at infrared wavelengths (Tomaselli et al., 1981), it was held constant to better illustrate the effects of particle size. Calculations were made for two log-normal size distributions, one with a geometric mean radius of 0.1 μm, and the other with a mean radius of 1.0 μm. The smaller value was chosen as typical of aerosol distributions produced by anthropogenic activity (Lenoble and Brogniez, 1984). The larger radius was chosen as typical of coarse aerosol distributions, typically produced by mechanical processes such as wind blowing across sand or soil; it also represents an approximate upper limit for a size distribution of climatic interest, since aerosols of larger sizes have atmospheric lifetimes of several days or less. In both cases the geometric standard deviation of the size distribution (a measure of the dispersion of particle sizes about the mean) was taken to be 2, which is typical of atmospheric aerosol distributions. For the smaller size distribution, absorption is fairly constant,although decreasing slightly with increasing wavelength, throughout the solar spectrum. At a wavelength of 1 μm, Q_e and Q_a both

decrease abruptly, and are reduced by more than an order of magnitude at 10 μm. For the larger particles, the peak absorption occurs at a wavelength of about 2 μm, although to a good first approximation, the absorption is fairly uniform from 0.3 to 5 μm. At a wavelength of 10 μm, the absorption efficiency is about half its value at a wavelength of 0.5 μm.

Another useful quantity, particularly from an experimental point of view, is the specific absorption, s_a. It is defined as the absorption cross-section per unit mass of absorber and is usually given in units of m^2/g. For homogeneous spheres, it is related to the absorption efficiency by the expression

$$s_a = \frac{(3/4)Q_a}{r\rho} \tag{3.2}$$

where r is the radius of the sphere and ρ is the density of the sphere. For x much less than 1 (i.e., small particles), absorption is directly proportional to the mass of the particle, which means that for a fixed wavelength, Q_a increases in direct proportion to r, the particle radius (because Q_a is equal to the absorption cross-section—which is increasing as r^3—divided by the geometric cross-section—which is increasing as r^2). Thus, from equation 3.2 above, s_a is independent of particle size for small absorbing spheres.

3.6.2 Absorption by Soot Agglomerates

Typical carbon aerosol agglomerates produced by combustion processes have mean radii on the order of a few tenths of a micron (Janzen, 1980; Borghesi et al., 1983). If these agglomerates were solid spheres of the same dimension and, thus, Mie theory were applicable, then, as illustrated in Figure 3.3, the particles would have a maximum extinction efficiency at visible wavelengths (see also Bergstrom, 1973; Faxvog and Roessler, 1978), and a very much lower efficiency at infrared wavelengths. In high density smoke plumes, the particles can agglomerate to sizes comparable to the wavelengths of infrared radiation or larger. Again applying Mie theory, these agglomerates would have reduced extinction efficiencies at visible wavelengths and increased efficiencies at infrared wavelengths.

However, Mie theory does not apply to agglomerated particles in general, and to fluffy or chained agglomerates composed of highly absorbing material such as soot in particular. While the scattering from these fluffy agglomerates would be similar to that from a solid object with the same dimensions, the absorption would be very different. Intuitively this may be understood by realizing that absorption of electromagnetic radiation is related to both the mass of the absorbing material and the amount of that mass which can be "seen" by an individual photon. Thus, for a fluffy object, which has a much greater surface to volume ratio than does a sphere of the same

size, much more of the absorbing material is available for interaction with the radiation. This effect may enhance the absorption of solar radiation by the agglomerated particle since each small carbon spheroid composing the agglomerate may act as an independent absorbing particle. Furthermore, because the spheroids in the agglomerate have only a minimal area of contact with each other, they cannot act as a volume absorber for radiation whose wavelength is much greater than their size.

This intuitive picture of absorption is supported to some extent by measurements of smoke absorption by laboratory smokes, but it needs further verification. Laboratory measurements of the specific absorption of soot agglomerates (e.g. Janzen, 1980; Wolff and Klimisch, 1982; Jennings and Pinnick, 1980; Roessler and Faxvong, 1980; see also Gerber and Hindman, 1982, for a detailed treatment of various measurement techniques and a report of an intercomparison experiment) consistently fall in the range of 8 to 10 m^2/g regardless of measurement technique or agglomerate size, supporting the picture of absorption outlined above. Lee (1983) carried out an extensive set of measurements of the specific absorption of a variety of carbon soot agglomerates. He also simultaneously obtained electron micrographs of the agglomerates. His results show that the specific absorption is independent of agglomerate size or shape until the agglomerates become very compact, i.e., they begin to resemble solid objects. Even in this case, however, the absorption is greater than that of a solid sphere of the same size. The results of measurements of spectral transmission between 0.5 and 2.2 μm reported by O'Sullivan and Ghosh (1973) are mixed. In experiments designed to study coagulation, they found a small decrease in optical density at 0.5 μm relative to 2.2 μm after 10 minutes of aging. This would be the expected result if larger particles were created through coagulation and Mie theory were applicable to these particles. On the other hand, their measurements of optical density for several different smoke concentrations indicate no change in the ratio of transmission at 0.5 to 2.2 μm, which may be due to insufficient time for coagulation to occur. Since these measurements do not distinguish between absorption and scattering, the change in absorption with aging cannot be directly deduced. Similarly, the results of Bruce and Richardson (1983) are inconclusive. They found that the specific absorption of soot at 10 μm was the same whether or not large aggregates were excluded, i.e., the large aggregates had the same absorption per unit mass as did small chains of carbon spheroids. Unfortunately, the relative abundance of large and small agglomerates was not carefully controiled in the experiments. Based on estimates from electron microscopy, they concluded that the large particles may have had insufficient mass to affect the reflectivity of their samples. Thus, they may also have been insufficient to have a detectable impact on the absorption.

Theoretical treatments of the spheroid problem (Jones, 1979; Berry and

Percival, 1985) support the picture that spheroids in chained or fluffy agglomerates act essentially as independent absorbers. However, these treatments are only approximate and further development is needed. Additionally, the problem of chains or fluffy agglomerates surrounded by approximately transparent liquids needs to be addressed (see discussion below). These latter particles actually may be dominant in the smoke from large fires. Clearly, there is a pressing need for further measurements of the optical characteristics, both absorption and scattering, of particles produced in smoke plumes.

3.6.3 Scattering and Absorption by Smoke

The discussion thus far has concentrated on particles consisting only of a single absorbing material. However, particles emitted from fires are composed of a variety of materials with varying optical properties. Several approaches for determining the optical properties of the composite smoke have been tried. The simplest is to assume that the optical properties of the composite are mass-weighted averages of the optical properties of the individual components. This approach is particularly attractive for smokes where the emitted materials can be broadly separated into amorphous elemental carbon, which dominates the absorption, and all other materials, which scatter light only. (This approach is *not* the same as taking a mass-weighted average of the indices of refraction of the various materials and then computing the specific absorption of the mixture from the average index of refraction. Such an approach is almost certainly incorrect for mixtures of highly-absorbing and weakly-absorbing materials.)

As noted above, the specific absorption of elemental carbon is well represented by the figure of 10 m^2/g. A number of other studies (e.g., Waggoner et al., 1981; Tangren, 1982) suggest that the specific scattering, s_s, of submicron particles is about 3.5 m^2/g at visible wavelengths between 0.5 and 0.6 μm. Thus the specific scattering and absorption of smoke may be approximated by the expressions

$$s_s = 3.5 \text{ m}^2/\text{g smoke} \tag{3.3a}$$

$$s_a = 10 f_{EC} \text{ m}^2/\text{g smoke} \tag{3.3b}$$

where f_{EC} denotes the mass fraction of elemental carbon in the smoke. Given the total mass of smoke emitted, the mass fraction of elemental carbon, and the area covered by the smoke, these expressions can be used to deduce the optical depth of the smoke and the attenuation of the solar radiation impinging on the smoke (see section 3.7)

The expressions (3.3a) and (3.3b) are based primarily on measurements of submicron aerosols. Observational studies of smoke from forest fires

(e.g. Radke et al., 1978; Tangren, 1982; Vines et al., 1971; Patterson and McMahon, 1984), small flaming sample fires (e.g. Bankston et al., 1981), and large 1000 MW fuel oil burners (Radke et al., 1980a) show that particulate matter in the submicron size range was produced in these fires. The production of much larger particles, however, has also been reported. Hobbs et al. (1984) recently measured the presence of a substantial mass fraction of particles with radii larger than 1 μm from prescribed burns of forest products. The measured number concentration peak was, however, at 0.1 μm. Similar observations of large particles produced by forest fires were made by Bigg (1985). Large agglomerates of soot particles can also be produced from surface oil fires (Day et al., 1979) and have been observed in urban environments (Russell, 1979). The burning of synthetic polymers can also produce large, supermicron sized, branched soot agglomerates (W.D. Woolley, J.E. Snell, personal communications). As discussed in the preceding section, (3.3b) may well be applicable to almost pure soot agglomerates in this case, provided that they are fluffy and not tightly packed. The applicability of (3.3a) for large, supermicron sized particles has not been justified.

If the smoke particles actually consisted of agglomerates surrounded by oil or water shells, as is typical of wood smoke for example, the optical properties of the particle could be modified by the presence of the shell, although the exact nature of this modification is not known. It is possible that the surface tension of the liquid would collapse the fluffy agglomerate into a more compact, roughly spherical particle. Calculations of the effect of a homogeneous, spherical shell of nonabsorbing material surrounding a concentric core of absorbing material show that the presence of the shell increases the absorption per unit mass of the core material by as much as a factor of 2 or 3, depending on the relative sizes of the core and the shell (Ackerman and Toon, 1981). A second possibility is that the agglomerate would break up into its component spheroids and that they are dispersed more or less uniformly through the nonabsorbing liquid. Calculations carried out for this case show an even more dramatic increase in the specific absorption (Chylek et al., 1984).

It is not entirely clear which of these models is correct either for the fresh smoke plume, where organic liquids may be condensing on the soot agglomerates, or for the plume at somewhat later stages where water may be condensing on the agglomerates. Limited experimental evidence exists for both (Chylek et al., 1984; Z. Levin, personal communication). To some extent, the appropriate model may be dependent on the material comprising the agglomerate and the forces holding it together, as well as the amount of water and/or organic liquids available to condense on it. However, according to the theoretical calculations, in either case the presence of a liquid deposit on an agglomerate would act to increase the effective absorption of the carbon, so that (3.3b) could strongly underestimate the absorption of

absorbing and non-absorbing aerosol. On the other hand, if the liquid were to evaporate, the residual aerosol particle would be more compact than the original fluffy agglomerate. It would also likely be increased in size, since more than one aerosol particle could be scavenged by the drop. Both these effects would tend to reduce the specific absorption of the elemental carbon as well as the lifetime of the particle. The magnitude of the reduction would depend on the final shape and size of the "processed" aerosol.

Experimental evidence bearing on the problem is ambiguous. The results of Patterson and McMahon (1985a,b), which were discussed in section 3.4, show no enhancement of specific absorption in wood smoke, suggesting that the theoretical models may be incorrect. However, no particle sizing or electron microscopy was performed, so the particle morphology in their smoke samples is unknown. On the other hand, comparisons of measurements of inferred elemental carbon concentrations (Rosen and Hansen, 1984) and of solar absorption (Ackerman and Valero, 1984) in Arctic haze events do suggest an enhanced specific absorption. Again, however, a complete description of particle size and composition was not obtained.

3.6.4 Wavelength Dependence

In order to assess the climatic impact of the smoke (as is considered in Chapters 4 and 5), it is necessary to know the value of the extinction and absorption at thermal infrared wavelengths as well as at solar wavelengths. Unfortunately, it is difficult to measure these properties at infrared wavelengths, so much of the available information is inferential or qualitative.

The calculations of Turco et al. (1983) and Ramaswamy and Kiehl (1985) for equivalent spheres give ratios of the extinction efficiency at 10 μm to that at 0.5 μm of about 1 to 10 or 15, and ratios of the absorption of about 1 to 5. The latter ratio is somewhat larger because a greater fraction of the extinction is due to absorption at infrared wavelengths. The transmission measurements of O'Sullivan and Ghosh (1973) and Randhawa and Van der Laan (1980) suggest this ratio may be as low as 1 to 100 for some smoke. Since aerosol extinction optical depth is directly proportional to the extinction efficiency, these values indicate that the optical depth of smoke at solar wavelengths is substantially greater than the optical depth at infrared wavelengths (which is true in general for atmospheric aerosols).

Qualitative information on the wavelength dependence of optical depth, and extinction efficiency, in actual fire plumes can be inferred from satellite imagery. Multiple views of the same scene taken with different spectral bandpasses show clearly visible smoke plumes from wildfires and agricultural burning at a wavelength of 0.5 μm, barely visible plumes at a wavelength of 3 μm, and no plume at all at a wavelength of 10 μm (Matson et al., 1984; J. Brass, personal communication). In fact, several research projects

currently underway are attempting to take advantage of the transparency of the plume at infrared and near infrared wavelengths to locate and monitor wildfires.

There are essentially no data available on the thermal infrared properties of urban smoke. Further research on both laboratory aerosols and fire plumes is urgently needed to quantitatively define the wavelength dependence of smoke extinction and absorption.

Some comments (e.g., Bigg, 1985) on the "nuclear winter" hypothesis have suggested that the infrared optical depth of smoke could be equal to or greater than the solar optical depth as a result of the production of large particles by coagulation. As evidence of this, the observation of the blue Sun in Europe in 1950 (Bull, 1951) is often cited. This effect was produced by the presence of atmospheric aerosols from Canadian forest fires (Wexler, 1950).

Typically, the Sun is red when viewed through fresh smoke plumes because the relatively small particles formed in the combustion process are more effective at scattering shorter wavelengths (blue light) than longer wavelengths (red light), while their absorption is roughly constant. Thus the Sun seen in transmission appears red. As the plume ages, the particles coagulate up to larger sizes which are approximately equally efficient at scattering all visible wavelengths. When viewed through this more aged smoke, the Sun appears white, or perhaps light grey, depending on the optical thickness of the plume. By extension, it has been suggested that the blue color of the Sun was due to the presence of very large particles (with radii on the order of 1 to 10 μm or larger (Bigg, 1985) formed by further coagulation in the plume as it travelled from Canada to Europe. Furthermore, measurements of atmospheric turbidity taken in Edinburgh showed that the plume had a somewhat larger optical depth at 0.6 μm than at 0.4 μm (Wilson, 1950). However, Porch et al, (1973) and E.M. Patterson (personal communication) has pointed out that the blue Sun and the measurements can be explained by assuming that the plume was composed of a very narrow size distribution of particles having a number mean radius of 0.5 μm. Considering the long distance which these particles travelled without experiencing gravitational settling, it seems more plausible that they were particles of this size rather than particles with radii on the order of 10 μm, as has been suggested by others.

3.7 ATTENUATION OF VISIBLE LIGHT

The emissions given in Section 3.3 and the optical coefficients given in Section 3.6 can be combined to provide an estimate of the effect of the smoke on sunlight reaching the ground. The average column density, D_c, (defined as the total mass of smoke in a vertical column with a cross-sectional area

of 1 m^2) of the smoke can be found by dividing the total smoke emission by the area over which it is assumed to spread. If the smoke is assumed to spread over half of the Northern Hemisphere (an area of about 1.28×10^{14} m^2), the average column density for the NRC emission estimate is 1.2 g/m^2, and for the CGB emission estimate is 0.4 g/m^2. In both cases, the average column density of amorphous elemental carbon would equal 0.23 g/m^2.

The extinction optical depth, τ, which is a dimensionless measure of the opacity of an atmospheric column, is the sum of the scattering optical depth, τ_s, and the absorption optical depth, τ_a. It can be computed from the expression

$$\tau = s_e D_c = (3.5 + 10.0 f_{EC}) D_c \tag{3.4}$$

where the right-hand side is found from the sum of (3.3a) and (3.3b). By definition, the first term on the right is τ_s and the second τ_a. Substituting the values of f_{EC} from section 3.3 and the values of D_c gives values of τ_s and τ_a of 4.1 and 2.3, respectively, for the NRC scenario and 1.5 and 2.3, respectively, for the CGB scenario.

The transmission of the direct solar beam through a column with optical depth τ is found from the expression $e^{-\tau}$, assuming the Sun is directly overhead, i.e., at the zenith position. (For the Sun at an angle θ from the zenith, the optical depth must be multiplied by secant(θ)). Under these conditions, even for the Sun at the zenith, the total sunlight, both direct and scattered, reaching the Earth's surface would be reduced to less than $e^{-2.3}$, i.e., less than 10%, of its normal value in both scenarios.

The actual amount of sunlight reaching the ground would be even less than that given above due to scattering by the aerosols. Sagan and Pollack (1967) derived an approximate formula for an effective absorption optical depth, τ_{eff}, that accounts for the combined effects of scattering and absorption:

$$\tau_{eff} = 1.7(\tau_a + 0.15\tau_s) \tag{3.5}$$

Although this expression was derived for optically thick atmospheres, it serves as a useful approximation in this context and was applied by CGB. Equation (3.5) gives the values $\tau_{eff} = 5.0$ for the NRC scenario and $\tau_{eff} = 4.3$ for the CGB scenario. These values imply a transmission of at most 1% of sunlight to one quarter of the Earth's surface due only to the smoke emissions.

This analysis of solar transmission through the atmosphere is only approximate and mainly descriptive. A more rigorous treatment of radiative transfer in smoke clouds can be found in Chapter 4, as well as in Turco et al., (1983a) and Ramaswamy and Kiehl (1985). In addition, it would take

some time for the smoke to be distributed over one quarter of the Earth. During this time, coagulation, rainout, and other microphysical processes would reduce the smoke levels in the atmosphere. These factors and their implications for the climatic impact of the smoke are discussed in detail in Chapters 4 and 5.

3.8 DUST

3.8.1 Formation Mechanisms

Ever since the first nuclear test explosion in the desert of New Mexico on July 16, 1945 (the Trinity test), scientists have realized that nuclear explosions can raise large quantities of soil dust and debris to high altitudes. The dust forming mechanisms are manifold (Glasstone and Dolan, 1977):

1. The thermal radiance of the fireball causes rapid steam expansion and blowoff of surface soil over a large area.
2. The blast winds and turbulence churn up additional soil and dust in the region adjacent to the burst.
3. Detonations on land surfaces eject large amounts of soil at high velocity during crater formation.
4. The high temperatures and pressures of the fireball in contact with the surface cause soil and rock to vaporize and liquefy; some of the material later solidifies into fine glassy aerosols.
5. The ascending fireball lifts entrained materials to high altitudes.
6. The suction and afterwinds created by the rising fireball draw additional dust and debris up the stem of the mushroom cloud.

3.8.2 Quantities and Properties

Based on analyses of dust samples collected in nuclear explosion clouds during the test series of the 1950s and 1960s, it has been estimated that, on average, 100,000 to 300,000 tonne of soil debris can be lofted into the stabilized cloud of a 1 Mt surface explosion (Rosenblatt et al., 1978; Gutmacher et al., 1983; NRC, 1985). Although most of the debris consists of particles exceeding 10 μm in radius, up to 5 to 10% (by mass) may consist of submicron particles (Nathans et al., 1970a; Yoon et al., 1985).

Information on the sizes of dust particles is sparse. For continental land surface explosions, data from the Johnny Boy near-surface test (Nevada Test Site, 0.5 kt, July 11, 1962) provide the most complete description of size distributions (Nathans et al., 1970a; Yoon et al., 1985). In this case, the size characteristics of the particles were carefully analyzed in the laboratory from filter samples collected in the stabilized explosion cloud. In this regard, it

should be noted that size distributions derived from fallout samples are not characteristic of the dust in the clouds aloft, particularly in the particle size range below several microns in radius. Data on the size distributions of dust raised by large nuclear tests on Pacific coral atolls are also of limited usefulness because of the small extent of the land masses and lack of continental soils at these sites. The Pacific tests seem to place a lower limit on the submicron dust mass fraction of about 1% (Heft, 1970). The uncertainty range in the submicron particle fraction for bursts on continental soils is at least a factor of three.

Following the largest atmospheric nuclear tests of the 1950s and 1960s, no obvious long-term effects from aerosol injection into the atmosphere were noted (e.g., Machta and Harris, 1955). This is not unexpected for several reasons:

1. In total, the principal tests amounted to about 450 Mt distributed over the decade from 1952 to 1962.
2. The largest tests occurred well above the surface, or on barren atolls, where minimal quantities of fine dust and essentially no smoke were produced.
3. The debris clouds were not carefully tracked and characterized, which precludes a present-day calibration of the expected effects.

The quantity of dust lofted by a nuclear explosion decreases steadily as the height-of-burst increases. As long as the fireball is in close contact with the surface, more than 100,000 tonne of debris can be lifted per Mt of explosive (the mass raised per unit yield decreases slowly as the yield increases above approximately 1 Mt). For a near-surface burst, in which the fireball is barely in contact with the surface, the amount of dust lofted is much smaller; in this case there is little vaporized material in the fireball and most of the dust is swept up by afterwinds. At even greater heights-of-burst, only the refractory materials used in bomb construction are available to condense as a fine aerosol (Nathans et al., 1970b).

For subsurface explosions, the amount of soil excavated from the crater at first increases with the depth-of-burst, then decreases again. However, while the quantity of soil displaced by a subsurface explosion may be greater (at some burst depths) than the quantity displaced by a surface explosion, the height of the dust cloud in the former case is lower because the fireball rise is damped in the denser medium. This also occurs in subsurface water bursts.

The heights of stabilization of nuclear dust clouds depend on the explosion yield, height-of-burst, season, and meteorological state of the atmosphere (Glasstone and Dolan, 1977). For low-altitude explosions of less than 100 kt, the stabilization height of the cloud depends to a large degree on the thermal stability of the lower atmosphere; the clouds can rise as high as the tropopause, but generally cannot penetrate into the stratosphere. For

surface and low-altitude explosions on the order of or greater than 100–200 kt, the cloud stabilization height is determined almost entirely by the thermal structure of the stratosphere. The cloud of a 1 Mt explosion at middle latitudes stabilizes wholly within the lower stratosphere; larger bursts stabilize at higher altitudes. In this dynamical regime, the height of stabilization scales approximately as $Y^{0.2}$, where Y is the yield in megatons (NRC, 1985). For long-term climatological studies, primary interest centers on the quantity of fine dust injected into the stratosphere (and perhaps the upper troposphere when the atmosphere is disturbed). Hence, surface and near-surface detonations on the order of or greater than 100–200 kt should be considered.

The morphology of nuclear-generated dust particles is diverse. The smallest particles (micron to submicron sizes) can be either spherical glassy (or metallic) beads or equidimensional soil and rock mineral grains. Spherical particles are produced by the condensation of vaporized refractory compounds and by the atomization of jets of liquefied minerals. Fine soil grains are produced by the crushing, disaggregation and entrainment of earth and rock. For optical calculations, the fine dust particles may be treated as equivalent-volume spheres. In the Johnny Boy dust sample, the specific extinction of the submicron particle fraction (at a wavelength of 550 nm) was about 3 m^2/g (NRC, 1985); the absorption is usually assumed to have accounted for 1–3% of the extinction (the remaining extinction being due to scattering).

There is conflicting evidence from the inspection of filter samples concerning the agglomeration of dust particles in nuclear clouds. While the clouds do not appear to be strongly electrified, they are highly turbulent and can hold substantial masses of ice (up to several hundred thousand tonne of ice per megaton of yield, from ground water and air moisture). Thus, turbulent coagulation and collection on ice crystal surfaces are possible aggregation mechanisms. Unfortunately, reliable quantitative information on dust particle clustering is unavailable. An early study pointed to the absence of agglomeration (Nathans et al., 1970a). However, a preliminary visual reanalysis of several high-altitude filter samples reveals occasional clusters of impacted particles (G. Rawson, personal communication). Whether these clusters are related to the breakup of true dust agglomerates, or are caused by the natural "shedding" of small particles by large soil grains upon impact (Rosinski and Langer, 1974), and what fraction of the total fine particle load is associated with agglomerates are unanswered questions. It is particularly noteworthy that the local fallout from surface bursts contains negligible quantities of submicron dust; indeed, 40–60 percent of the total radioactivity carried by the finest dust grains escapes into the global atmosphere (Glasstone and Dolan, 1977). In view of the existing evidence, submicron particle agglomeration in the early stabilized clouds

of nuclear surface detonations may be treated as a secondary effect, although long-term coagulation and removal of the dust must be accounted for (Turco et al., 1983a,b).

Since most of the nuclear test explosions were conducted on barren soils, little is known about the impact of soil organic matter on dust cloud optical properties. In fact, many potential targets of surface nuclear explosions, particularly missile silos, are based in regions of highly organic soil (e.g., the chernozems of the U.S. Great Plains and the peat soils of the Siberian forests). In some locales, the soils are black. The aerosols formed from these organically rich soils could strongly absorb sunlight. Any of this organic material engulfed in the fireball would be largely oxidized (burned), but some of the organic material scoured up by the blast and afterwinds would not be burned and could potentially absorb a significant fraction of the incident sunlight. By contrast, aerosols generated from barren soils are unlikely to absorb sunlight efficiently (although, occasionally, the finest glassy particles collected in nuclear clouds are black due to dissolved iron compounds). In the climate calculations carried out to date, the aerosols have been assumed to be only weakly absorbing.

Most of the nuclear tests were also conducted over coarse soils (e.g., coral atolls), whereas most nuclear targets are located in soils with substantial clay (fine particle) fractions. (The Johnny Boy test, however, occurred on a desert alluvium with a substantial fine particle abundance; G. Rawson, personal communication.) Finer parent grain sizes imply that greater quantities of submicron dust can be generated when the soil is dried and pulverized by a nuclear burst.

A number of factors could reduce the quantity of dust lofted by a surface or near-surface nuclear detonation:

1. Soil moisture, which increases soil cohesion.
2. Vegetative cover, which blocks thermal radiation and holds soil down.
3. Surface layers of hardpan, rocks, snow, or ice, which suppress dust formation.

On the other hand, vaporization and liquefication of the soil, and pulverization of surface materials within the high-overpressure "sweep up" zone, should not be greatly affected by these factors.

3.8.3 Multiburst Effects

Nuclear attack strategies may call for multiple targeting of key military facilities (for example, double or triple detonations over missile silos). Explosions that are proximate in both space and time will interact strongly. However, there are no nuclear test data bearing on "multiburst" processes. The following effects might be expected:

1. An initial explosion would dry, excavate, and pulverize soil, which then could be more easily swept up by subsequent explosions.
2. Overlapping fireballs would reinforce buoyant motions, carrying dust to greater altitudes than might otherwise be expected (in order for reinforcement to occur, the weapons would have to be detonated within seconds of each other at nearly the same location, a feat that might be difficult to achieve operationally).

Only preliminary hydrodynamic model calculations are available to estimate the effects of interacting nuclear bursts (e.g., Filipelli, 1980; NRC, 1985). The calculations suggest a potential enhancement in dust lofting. One analysis argues on physical grounds that the dust mass raised (per megaton of yield) could be larger by a factor of 10 in multiburst environments (NRC, 1985), although detailed quantitative demonstrations of this point are lacking.

3.8.4 Integrated Dust Injections

Figure 3.4 shows a simulated dust pall that could be generated in a counterforce nuclear exchange between the superpowers (Yoon et al., 1985). The predicted total quantity of submicron dust in the upper atmosphere after 5 days resulting from 2500 Mt of land surface bursts is 40 million tonne. This is about twice the quantity computed by the NRC (1985), about one-half the baseline quantity of Turco et al. (1983), and roughly the quantity expected from the scenario outlined in Chapter 2. The differences in dust injections can be attributed mainly to differences in the assumed total yield of surface bursts. The simulation in Figure 3.4 assumes a dust mass lofting (for surface explosions) of 0.27 million tonne per megaton of yield, with about 8% of that amount in the submicron size range. Roughly one-half of the dust is generated by explosions in the yield range of 2–20 Mt, and one-half by explosions in the range of 0.3–2 Mt. Given the current evolution of weapon yields toward the smaller range, the amount of dust and the height of injection may be somewhat too large in this simulation, but the general features of the simulation would still be appropriate.

The dust simulation of Yoon et al. (1985) suggests that, after just 5 days, the initial, stabilized detonation clouds would have been displaced and sheared by the prevailing wind systems, and would blanket most of the northern mid-latitude zone under a pall of soil debris. The extinction optical depths at visible wavelengths, most of which contributes to scattering, are greater than 8 in some regions, although, if the dust were distributed uniformly over the Northern Hemisphere, the optical depth would be 0.5. While, for a given optical depth, the radiative effects of dust are considerably smaller than the radiative effects of smoke, an optical depth of 8 can reduce the average solar energy reaching the ground by 80 percent (see also Chapters 4 and 5).

Figure 3.4. Geographical distribution of nuclear dust clouds five days after a July counterforce exchange of 4000 Mt against missile silos and air bases. A three dimensional tracer model was used to follow the dispersion of the dust clouds. Winds for July were obtained from the 2.5° grid data of the National Meteorological Center, Washington, DC, and were updated every 12 hours in the simulation. The (zenith) extinction optical depth contours (for $\tau = 0.32$, 1.5, and 7.7) at a wavelength of 0.55μm are given. Essentialy all of the dust in the figure resides in the upper troposphere and stratosphere. The particle physics treated in the model is described by Yoon et al. (1985). (Figure supplied by B. Yoon.)

The data in Figure 3.4 may represent a reasonably conservative picture of the dust environment after a major nuclear exchange. For example, the calculations could also take into account a broader range of military targets, higher absorption by the aerosol due to the organic component of the soil, multiburst effects, and possible dust injections by powerful updrafts over intense fires. Factors that could limit the injection include early agglomeration and rainout and weather conditions favoring soil cohesion.

It should be noted that the injection of dust into the stratosphere is more important for the development of climatic effects than injection into the troposphere, because stratospheric dust has a much longer lifetime (in the unperturbed atmosphere). Owing to the uncertainties in the number of

surface bursts, the dust mass lofted, particle size distributions, and multiburst interactions, the total quantity and impacts of nuclear-generated dust will remain ambiguous. However, the quantities of optically-active dust raised by a full-scale nuclear exchange could, within the parameter ranges defined by observations, be large enough to cause some environmental disturbances even without smoke injection.

APPENDIX 3A

Urban Fire Development

3A.1 INTRODUCTION

No comprehensive analysis exists of large urban fires, either nuclear-initiated or of conventional origin. In previous global estimates of the extent of urban fires and the amount of smoke generated from a nuclear attack, it has been assumed that about 250 km^2 could be ignited and burned by a 1 Mt detonation (Turco et al., 1983a,b; Crutzen et al., 1984; NRC, 1985). This assumption can be checked by analyzing fire-development processes on local urban scales. In this section, three distinct types of urban areas are studied to assess fire ignition and spread characteristics:

1. An idealized "uniform" city, representing a continuous residential area with wooden, two-storey structures;
2. A predominantly suburban/residential area (with many vacant lots serving as firebreaks), represented by San Jose, California in the late 1960s;
3. A major industrial/urban area, represented by Detroit, Michigan in the late 1960s.

The uniform city is useful for extensive parametric studies and for possible applications to urban areas in which fuel distributions may be relatively uniform. Data from the 1960s are used for San Jose and Detroit because current data are not available.

In analyzing fire history in each individual urban area, the initiation and spread of fires is considered in detail. Firestorms and rubble-zone fires are not treated because of the very limited understanding of these phenomena. Nevertheless, such fires could be important after a nuclear war, and they are discussed in Section 3A.6.

3A.2 FIRE DEVELOPMENT IN A SINGLE URBAN AREA

To determine the amount of smoke generated in an urban area following a nuclear attack, a characterization is needed of the area burned, the rate of burning, and the fuel consumption, among other factors. For precise simulation, specific information such as the yield and burst point of the nuclear weapon, weather conditions, fuel distribution patterns, etc., is also

required. The physical factors and the chain of events required in fire spread modelling are shown in Figure 3A.1. A theoretical treatment should consider all of these factors. However, in the context of studying the after-effects of a nuclear war, it is possible that specific details of the fire development would be less important than gross factors such as the total fuel impacted.

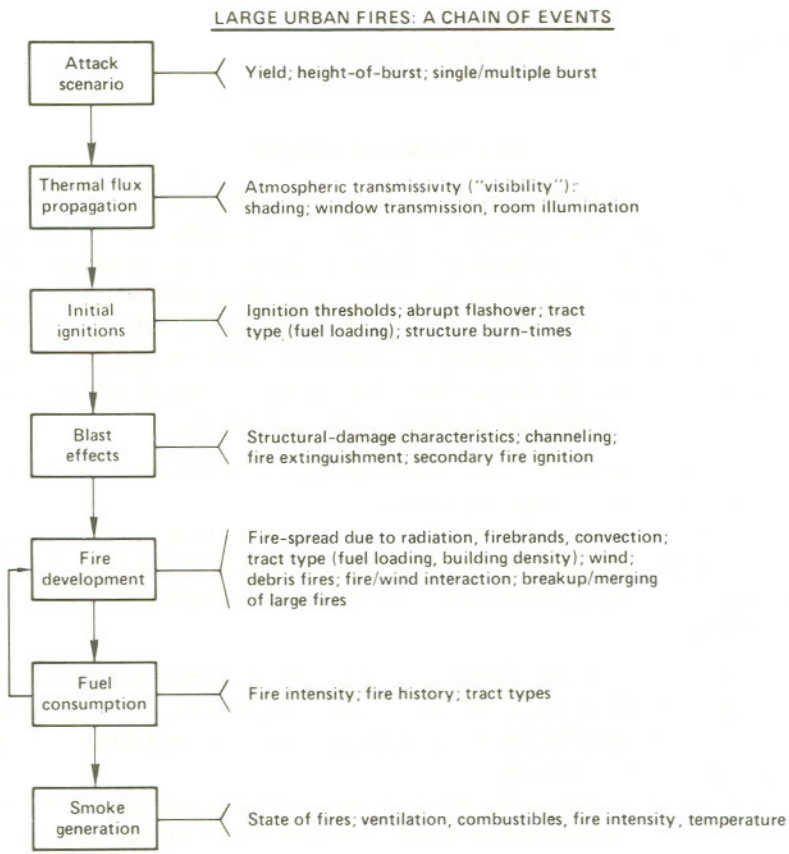

Figure 3A.1. Chain of events for characterizing urban fires and smoke generation

Physical models utilized to make urban fire calculations are described in detail by Kang et al. (1985), and references therein. Briefly, the models are based on empirical relationships between characteristics of urban buildings and fire development and spread. Clearly, such a model requires an enormous amount of data and physical knowledge of fires; not all of the needed information is adequately defined at this time. Nevertheless, the urban-fire model used by Kang et al. (1985) has been employed to provide insights into the kinds and scales of effects that might be expected in the aftermath of a nuclear explosion over a city. The results presented here should not be

interpreted as literal descriptions of post-nuclear-war fire conditions. For example, the model does not include the important components of stored fossil fuels (petroleum, gasoline, natural gas distribution systems, etc.) or asphalt in its fuel loading estimates, nor an itemization of fuel types (e.g., plastics, organochemicals, etc.). Many of the assumptions and caveats pertaining to these calculations are discussed by Kang et al. (1985). More general descriptions of the problem are given by Horiuchi (1972), Takata (1972), Wiersma and Martin (1975), Aoki (1978), Sasaki and Jin (1979), Takayama (1982), and Reitter et al. (1985).

The computational procedure used by Kang et al. (1985) can be summarized as follows. The urban area is divided into uniform, square tracts that are each relatively homogeneous with regard to type and density of structures; the tracts are separated by natural or man-made firebreaks (e.g., streets, rivers, or parks). Following the initial ignition of the area by a nuclear

TABLE 3A.1.
SOME MAJOR SIMPLIFICATIONS IN THE URBAN FIRE MODEL OF KANG ET AL. (1985)

- Tracts are small enough so that their built-up areas can be treated as homogeneous in a statistical sense.
- Tracts are large enough that ignition and fire spread can be treated probabilistically.
- Tracts can be idealized as squares, all the same size.
- Firebreaks between tracts are sufficiently large (at least 30.5 m) to prevent spread between tracts by radiation.
- Only one wall of a building is exposed to the fireball.
- Only interior fuels are important in ignition.
- Frequency of secondary (blast-caused) fires is proportional to floor area: one per 10^4 m^2 of floor space is assumed.
- Blast can extinguish primary fires at overpressures of 2 psi or greater.
- "Abrupt flashover" is neglected. ("Abrupt flashover" refers to the rapid ignition of an entire room exposed to large amounts of thermal radiation from a fireball.)
- Flashover of one room in a building leads to a sustained building fire.
- Building burning history is entirely based on the ignition of a single room, which occurs with equal probability on any floor. ["Building burning history" is the time a particular building type spends in active (flaming) combustion.]
- Building burning history is independent of moderate blast damage.
- There is no fire interaction between the debris and the non-debris regions.
- Ambient wind is constant throughout the fire area for total time of interest.
- Fire-induced aerodynamics are neglected.
- Wind effects upon the building fires and radiant fire spread are neglected.

detonation, a time-marching computational routine is employed to follow the fire-spread history. At each time step, empirically-derived probabilities are used to calculate the expected numbers of buildings ignited by radiation or by firebrands in each tract. Ignited buildings progress through several stages of burning, leading to the phase during which spread to other buildings can occur. The basic numerical model is based on work carried out by Takata and Salzberg (1968) and Takata (1972). Table 3A.1 summarizes the most important assumptions.

The overall results of many simulations (assuming a 1 Mt detonation) suggest that the dominant factors in urban fire ignition and spread in a nuclear attack are: the distance the thermal pulse can propagate and ignite fuels, fuel loadings, ambient windspeed, and firebrand production rate. The simulations for San Jose and Detroit showed additional dependence on the yield and point of detonation and the fuel-distribution patterns (as well as on the weapon yield). Details are given in Kang et al. (1985).

3A.3 UNIFORM-CITY CASE STUDY

A "uniform" city is assumed to be characterized by a single building type, a constant building density and fuel loading, and constant firebreak dimensions; each structure is assumed to have the same ignition and fire-spread probabilities. Table 3A.2 summarizes pertinent input conditions used for uniform city calculations.

Baseline calculation results are shown in Figures 3A.2 to 3A.5 for a 1-Mt burst at 3 km altitude above Ground Zero (denoted GZ). In the severely blast-damaged area (here assumed to be the area exposed to an overpressure greater than 3.5 psi = 24 kPa), fires could burn actively, smolder, or be entirely extinguished (if initially ignited), depending upon a number of complex physical processes, including the fuel to non-fuel debris ratio and the mixing characteristics of the fuels. For the current simulation, the fuel in the debris region is assumed to be "affected" by fire, i.e., the fuel could burn. Typically, in large fires, the fuel-consumption fraction is assumed to be 50% (Takata and Salzberg, 1968; Chandler et al., 1963); however, this value has not been firmly established. Any fuel not consumed in the first wave of burning could smolder for a longer period, sometimes for days if not extinguished. Because the fraction of fuel which burns rapidly (as against that which smolders or does not burn) is not known, figures for fuel are given in terms of the total fuel within the fire and the debris zones, representing the maximum available fuel in these zones (except for fuels not accounted for, as noted above, and subject to the uncertainties in the fuel loading estimates themselves).

In the non-debris area, the ignited structures serve as a source of subsequent fires within a tract through radiation and firebrands, as well as a

TABLE 3A.2
BASELINE CASE PARAMETERS FOR UNIFORM CITY

Attack Scenario:	Yield = 1 Mt, HOB = 3 km,	
Atmosphere:	Visibility = 19.3 km, Wind = 2.68 m/s (6 mph)	
Tracts:	Tract types	= 1 (uniform),
	Tract dimension	= 0.8 km × 0.8 km
	Building density	= 15%
	Density of built-up Areas	= 100%
Structures:	Wooden, residential, 2 stories	
	Height	= 5.9 m
	Window area/Wall area	= 0.1
	Window transmittance	= 0.7
Fuel:	Specific fuel loading	= 100 kg/m^2 of floor area
	Areal fuel loading	= 30 kg/m^2
Fire:	Lowest critical ignition energy	= 7.7 cal/m^2
	Secondary ignitions	= 1 fire per 10^4 m^2 of floor area
	Brand generation rate	= 18 per m^2 of roof area[a]
	Brand transport range	= 460 m
Blast effects:	Severe blast damage (debris) above 3.5 psi overpressure	
	Moderate blast damage between 2 psi and 3.5 psi	
	No blast damage below 2 psi	
	Secondary fires above 2 psi overpressure	
	Some primary fires extinguished above 2 psi	

[a] Calculated as total brands above a minimum size coming from an entire burning structure divided by the roof area.

source of fires to neighboring tracts by firebrands. Generally after several hours, the peak-burning rate is reached, involving areas initially ignited by the fireball and tracts subsequently ignited by firebrands. Figure 3A.2 shows the fire area at t = 25 hr after the explosion. Note that the fires leave behind a burned-out annular fire "ring" between the debris region and the fire front (which may in fact include the debris region).

The predicted area affected by fires as a function of time is given in Figure 3A.3. The initial affected area was approximately 510 km^2, of which about 40% was in the debris region. During the course of 25 hours of conflagration, the fire area outside the debris region increased to about 760 km^2. Figure 3A.4 illustrates the fire intensity, which reached a peak at approximately 5 hours after the burst and subsided to a steady, moderate level thereafter as the fire continued to spread. The fuel consumption was rapid in the first few

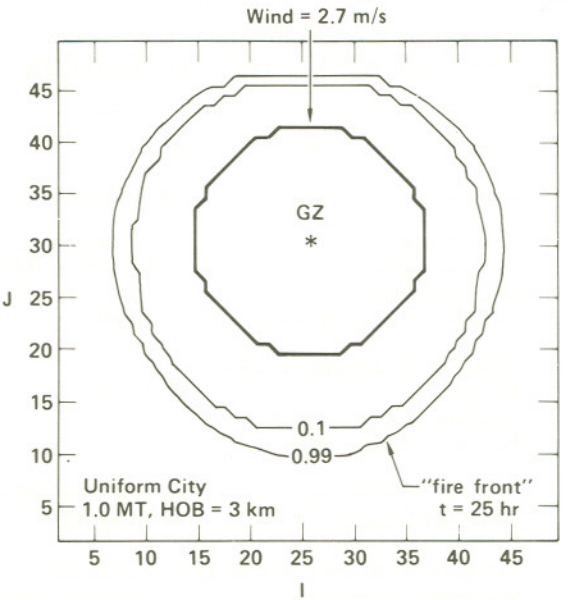

Figure 3A.2. Fires in uniform city at 25 hr after a 1-Mt detonation at 3 km altitude, baseline case (constant windspeed at 2.7 m/s). Each I, J coordinate refers to a 0.8 km × 0.8 km tract; the numbers on the contours denote the fraction of buildings still unignited

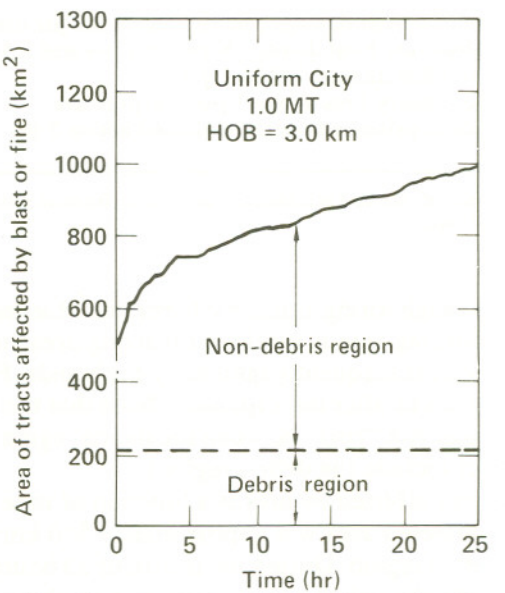

Figure 3A.3. Fire-affected area vs. time for uniform city, baseline case (1 Mt, 3 km HOB). For simplicity, the area of the entire tract is considered to be affected by the fire when at least one structure within it is on fire. Over time, virtually all structures in a tract will burn

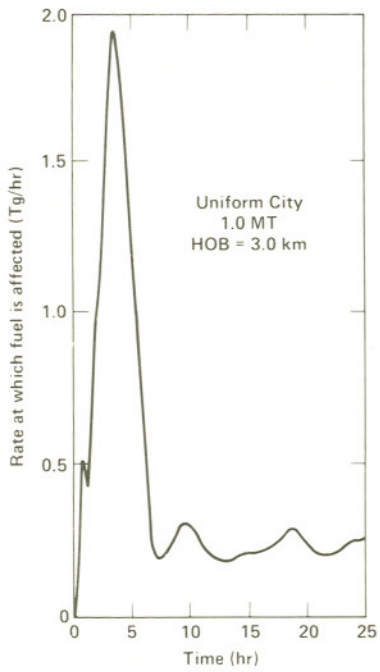

Figure 3A.4. Rate that fuel is engulfed by fire in the non-debris region in a uniform city, baseline case. A typical assumption is that 50 percent of this amount burns; this assumption is made in Kang et al.'s model

hours and then adjusts to a relatively constant rate, extending even beyond 25 hours due to spreading of the fires. The total cumulative quantity of fuel in ignited structures within the fire zone as a function of time is shown in Figure 3A.5; the fuel in the debris region is also included to emphasize the possible effect of fires there.

The results of an extensive sensitivity analysis of nuclear-induced fires in a "uniform" city are summarized in Table 3A.3. The dominant factors affecting the fire outcome are: ambient wind, atmospheric visibility, firebrand production rate, fuel loading, thermal-pulse ignition thresholds, and secondary (blast-induced) ignition frequency. All of these factors are subject to considerable uncertainty. The simulated dependence of fire behavior on each of them was, however, consistent with qualitative physical reasoning.

Fire characteristics for simultaneous bursts have also been calculated, but the detailed results were not presented here. When two well-separated 0.5 Mt bursts were detonated over the uniform city, and no interactions between the

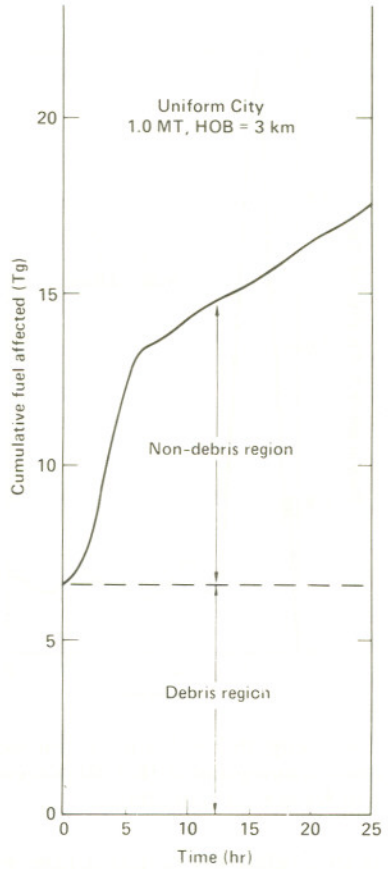

Figure 3A.5. Cumulative fuel in structures actually on fire as a function of time for uniform city baseline case (1 Mt, 3 km HOB). The total fuel in the fire zone at any time, including structures not yet on fire, would be greater. Of the total fuel for each structure, only a certain fraction would usually be consumed in active flaming. For the non-debris firespread region, it is usually assumed that 50% of the fuel is consumed in active flaming; the rest is usually assumed to be consumed in later smoldering. For the debris, burnout estimates vary from zero to 100 percent

fires were assumed, the total fuel affected increased by about 30% over the baseline 1-Mt case after 25 hours (including the debris areas). This result suggests a modest increase in fuel consumption for simultaneous smaller bursts, depending on their sizes and relative placement. (See also Chapter 1 for a discussion of incendiary efficiency for various yield weapons.)

TABLE 3A.3.
PARAMETER SENSITIVITY STUDY FOR IDEALIZED UNIFORM CITY (NON-DEBRIS REGION)

Parameter varied	Modification from baseline case	Fuel consumed normalized to baseline case		Normalized relative area[a]
		t = 5 hr	25 hr	t = 25 hr
Windspeed	x 2	1.30	1.23	1.18
	x 3	1.40	1.34	1.24
Firebrand generation rate	x 1/2	0.76	0.91	0.92
	x 2	1.40	2.08	1.11
Blast extent	2 psi	0.72	1.00	1.00
Visibility	12.9 km	0.67	1.00	1.00
	32.0 km	2.14	1.57	0.89
Secondary ignitions	x 2	1.42	1.02	1.01
	x 1/2	0.73	0.98	0.99
	0	0.43	0.85	1.04
Building density	x 2	1.45	1.19	1.13
	x 1/3	0.58	0.76	0.84
HOB	4.0 km	1.19	1.20	0.97
	3.5 km	0.96	1.01	1.00
	2.5 km	0.97	0.87	1.04
	2.0 km	0.97	0.82	0.99
Lowest critical ignition energy	10.4 cal/cm^2	0.74	1.00	1.00
	5.0 cal/cm^2	1.52	1.33	0.93
Window transmittance	1.0	1.76	1.18	0.97
	0.4	0.67	1.00	1.00
Specific fuel loading	x 2	1.41	1.08	1.04
	x 1/2	0.42	0.88	0.92
Window area	x 2	1.42	1.27	1.14
	x 1/2	0.65	0.72	0.86
Baseline case results:	Fuel consumed[b] outside debris region	= 4.8 Tg (5 hr) = 10.9 Tg (25 hr)		
	Total fuel affected	= 30.0 Tg (25 hr)		
	Area affected	= 226 km^2 (debris region) = 534 km^2 (non-debris; 5 hr) = 764 km^2 (non-debris; 25 hr)		

[a] This column presents the ratio of two ratios; i.e., the area affected at 25 hr divided by the area affected at 0 hr for the case with a varied parameter divided by the same ratio for the baseline case.

[b] 50% fuel consumption rate is assumed.

3A.4 SAN JOSE, CALIFORNIA (1968) CASE STUDY

San Jose, California of the mid-1960s represents a typical, predominantly suburban residential area. Extensive information is available from that time on the firebreaks, building types and fuel distributions (Takata, 1969, 1972). As a case study, a 1-Mt burst was assumed to be detonated at 2.4 km altitude over the southern tip of San Francisco Bay, north of San Jose. The choice of this GZ was made in the Five-Cities study, presumably to optimize blast damage to the military-industrial complex on shore nearby. Table 3A.4 describes the baseline parameters for this case.

TABLE 3A.4.
BASELINE CASE PARAMETERS FOR SAN JOSE AREA (1968)

Attack Scenario:	Yield = 1 Mt, HOB = 2.4 km, GZ at (I = 16, J = 33)	
Atmosphere:	Visibility = 19.3 km, Wind = 2.68 m/s (6 mph) from the west	
Tracts:	Tract types	= 14[a]
	Tract dimension	= 0.8 km × 0.8 km
	Total number	= 1428 (occupied = 699) tracts
Blast effects:	Severe blast damage (debris) above 6 psi overpressure Moderate blast damage between 2 psi and 6 psi No blast damage below 2 psi Secondary fires above 2 psi overpressure Some primary fires extinguished above 2 psi	
Fuel:	Total mass of fuel in area	= 3.05 Tg
	Fuel in residential tracts	= 5–11 kg/m^2
	Fuel in industrial tracts	= 21–88 kg/m^2
After attack:	Number of tracts initially involved (i.e., 55 blast-destroyed)	= 240
	(185 ignited)	
	Fuel available in debris area	= 0.31 Tg

[a] The tract types vary according to the built-upness of the area, the building density, and the building height and floor area. There are 8 residential tract types with a specified fuel loading of 50 kg/m^2-floor 2 industrial tract types with 88 kg/m^2, 2 school tract types with 24 kg/m^2, and 1 commercial tract type with 24 kg/m^2. The residential fuel loading may be low by a factor of two (Issen, 1980).

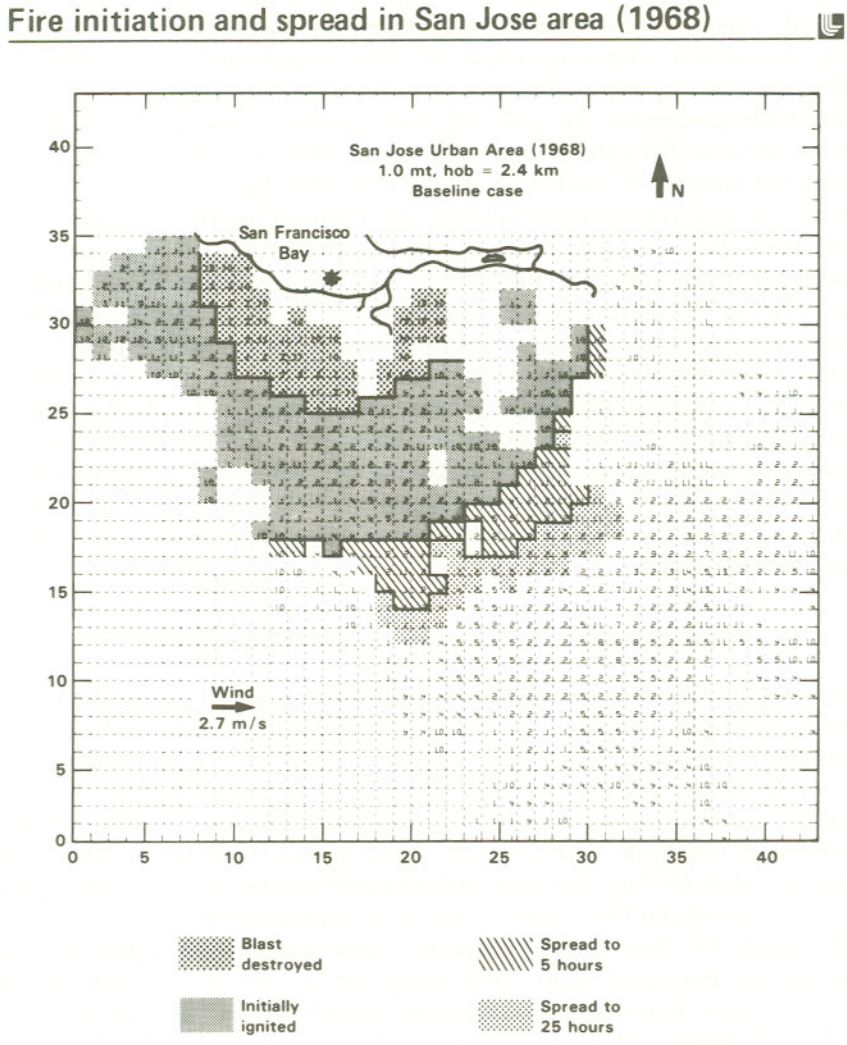

Figure 3A.6. Fires in the San Jose, California area assuming 1968 fuel load distributions (1 Mt at 2.4 km HOB)

Figure 3A.6 shows the ground zero, debris area, the fire ignition and spread patterns $t = 5$ hours and $t = 25$ hours after detonation. After 25 hours, the total area damaged and burned was calculated to be about 200 km^2 (even though the initial detonation occurred over the Bay and did

not ignite downtown San Jose). The majority of structures in San Jose are primarily residential, holding about 50 kg of fuel per square meter of floor space. (While this value may be low for current residential structures (Issen, 1980), the present calculation may be considered as a sample case study.) Under these conditions, the total fuel affected in the non-debris fire-spread region was about 0.5 million tonne (Tg) after 25 hours; in the adjacent debris region, the amount of available fuel was about 0.3 Tg.

When ground zero was moved from the Bay southward to include more of the developed area of San Jose (i.e., to 9.6 km southward of ground zero shown in Figure 3A.6), the total urban area initially affected increased to about 250 km^2 (91 for the debris region, and 156 for the ignited region), then slowly increased to about 260 km^2 after 25 hours, and to about 370 km^2 after 50 hours. The total fuel affected was about 1.5 Tg (1 Tg in the non-debris region; 0.5 Tg in the debris region). These results suggest that the fire history is "city-specific", i.e., the distribution patterns of a particular city and the specific nuclear targeting near or within the city influence the fire outcome. Thus, a reasonably detailed survey, especially of the fuel distributions, may be a prerequisite for predicting the potential time-dependent fire-spread in a specific urban area.

3A.5 DETROIT, MICHIGAN (1968) CASE STUDY

Many single-burst cases have been calculated for various GZ locations over Detroit, involving 1 Mt and 0.5 Mt weapons. For the 1-Mt cases, the height-of-burst (HOB) was assumed to be 2.6 km in order to maximize blast damage, while for the 0.5-Mt cases, a HOB of 2.1 km was assumed. The wind velocity was taken to be westerly at 4 m/s. Note that fuel loadings varied according to tract type, with 50 kg/m^2 (floor space) assumed for residential structures, as in the San Jose case, and 88 kg/m^2 for industrial tracts. Figure 3A.7 is a map of the Detroit area displaying various tract types.

The results for these single-burst cases varied widely according to the GZ location. For example, Figure 3A.8 shows the fire area for a 1-Mt blast at $t = 25$ hr after detonation, encompassing about 840 km^2 (which included 110 km^2 of debris region), and involving 14 Tg of combustibles (with about 2 Tg in the debris region). In the model, the fires continued to burn in the windward direction until firebreaks were reached, e.g., Lake St. Clair. No fuel data were available to consider fires in adjacent areas in Canada, and therefore ignition and firespread in that region were not considered. The results are summarized in Table 3A.5.

Multiple, near simultaneous burst effects were also considered as a possible attack scenario, but the precise results are not presented here. Figure 3A.9 illustrates the fire zones one-day after two 0.5 Mt weapons were exploded at different locations over Detroit. Interactions between the fires were

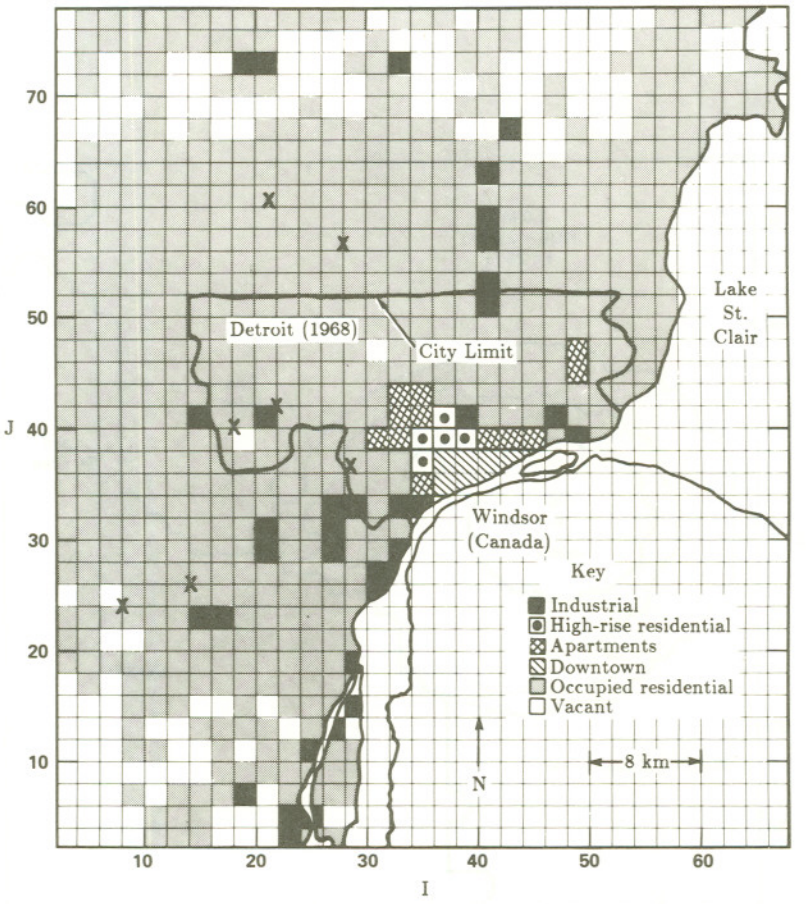

Figure 3A.7. Detroit, Michigan area fuel loading as of about 1968. Each I, J coordinate denotes a 0.8 km × 0.8 km tract; each **X** refers to a location that served as ground zero in a set of tests of the effects of a single detonation

ignored. The total area affected was about 1,370 km^2 (including 420 km^2 of debris region), a sizeable increase over the single-burst, 1-Mt case. On the other hand, the total fuel involved was somewhat lower at about 11 Tg (with 1.3 Tg in the debris region), because less-dense areas were burned up to this time. This again demonstrates the importance of the attack scenario and the fuel loading patterns. Note that the 11 Tg translates into an average fuel loading of about 8 kg/m^2, which is about the same as was assumed in the San Jose residential areas (Table 3A.4) and is also probably a low estimate.

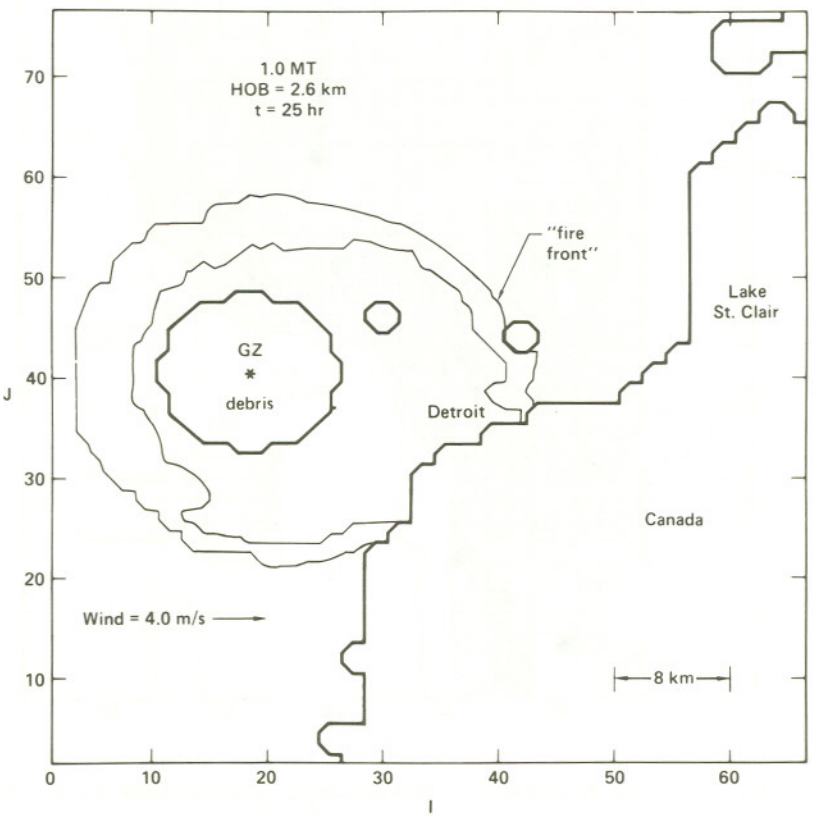

Figure 3A.8. Fires in the Detroit, Michigan area, assuming fuel loading characteristic of about 1968, 25 hours after a 1 Mt burst. Bold lines outside the debris region indicate fire breaks (e.g., water bodies, open areas)

Because the fraction of the total fuel in a city that becomes involved in the fire zone is also of interest, these have been calculated and are shown in Table 3A.5. The fractions of fuel affected by fires depend on many factors which are specific to the city in question. Nevertheless, it appears that a sizeable fraction of all the fuels in a major city, plus its suburbs, could be ignited by about 1 Mt of nuclear explosives (Table 3A.5).

Table 3A.5 Urban fire areas and fuel burdens for single detonations.

Case	Yield (MT)	Area of fire zones (km^2)			Fuel available in fire zones (Tg)			Fraction of total fuel in fire zones (Percent)[a]		
		Debris Region	Non-debris 25 hr	Non-debris 50 hr	Debris Region	Non-debris 25 hr	Non-debris 50 hr	Debris Region	Non-debris 25 hr	Non-debris 50 hr
Uniform City	1.0	226	764	1016	6.3	21.8	35.0		(*b*)	
	0.5	143	516	775	4.0	12.9	23.2			
San Jose[c]	1.0	91	156	275	0.5	1.0	1.1	15%	32%	36%
	0.5	59	148	251	0.3	0.7	0.9	8	22	31
Detroit[d]	1.0	91–109	610–733	714–911	1.7–4.4	11.5–13.1	14.2–18.0	6–17	45–51	56–70
	0.5	63–65	404–582	548–755	0.3–1.6	1.4–11.4	4.5–16.3	1–6	5–44	18–64

[a] When at least one structure is on fire, the entire tract is considered to be in the fire zone.
[b] For the uniform-city case, the fraction is not given because the total urban area is not specified.
[c] For the case with a ground-zero located 9.6 km south of the ground-zero shown in Figure 3A.6.
[d] The upper and lower figures give the range of values obtained for a number of simulated burstpoints.

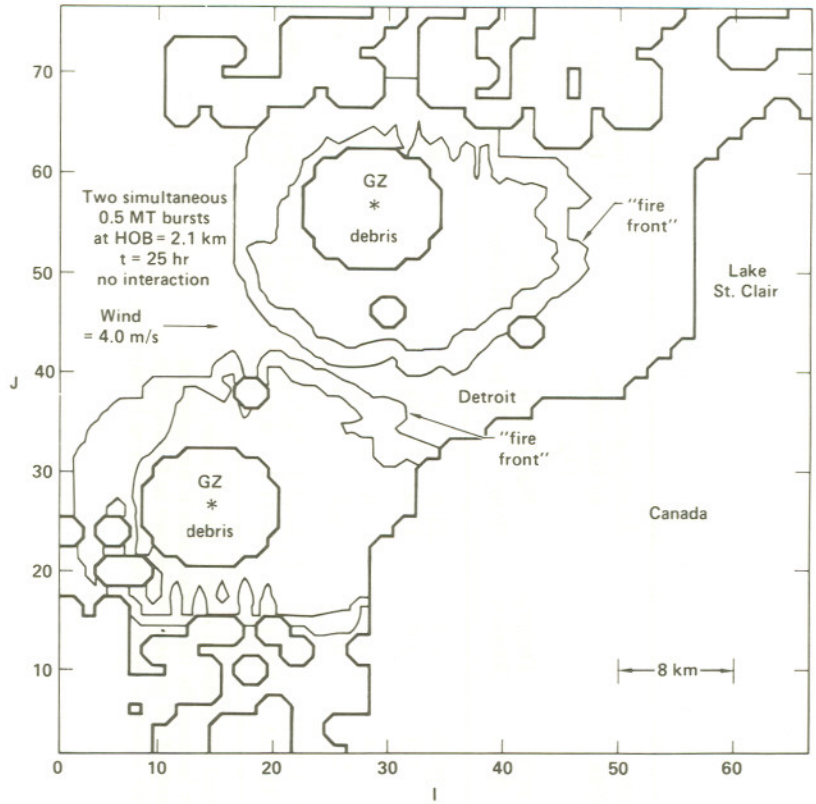

Figure 3A.9. Fires in the Detroit area, assuming fuel distribution characteristic of 1968 and for two simultaneous 0.5-Mt bursts, 25 hours after detonation. Bold lines outside debris regions indicate fire-breaks

3A.6 DISCUSSION

From the foregoing analysis, it is obvious that variability exists in the fire areas and the amounts of fuel consumed with differences between cities, and with burst location within a city, due mainly to variability in the fuel load and distribution. Nonetheless, based on these simulations several tentative conclusions may be reached. First, the dominant factors in fire spread are: fuel loading, reach of the thermal-pulse, ambient windspeed, and firebrand production rate. In addition, the cities with irregular fuel distributions display fire histories that are distinct from an idealized "uniform" city, with dependence upon the attack scenario and the fuel distribution patterns. Second, the potential burnout areas in cities under nuclear attack can be as large as 1000 km^2 after one day, when fire spread by the ambient winds is included.

These estimates do not take into account the likely significant role of liquid fossil fuels in stationary and spreading fires in urban/industrial zones. In the larger cities, the total fuel potentially involved in fires can range up to 20 Tg or more (Table 3A.5) after a day, although in sparse residential zones the value may be closer to one-tenth this figure. Indeed, a large-scale nuclear exchange could impact an enormous quantity of fuel, and presumably create large amounts of smoke (see Section 3.3).

A number of potentially important physical factors have not been included in the present calculations: synergistic effects of simultaneous fires, abrupt flashover (the Encore effect; see Chapter 1), merging and breakup of fires and plumes, fire-wind interactions, fire phenomena in the debris region, and firestorms. Fires in the debris region may burn actively, smolder, or be entirely extinguished, depending on the debris formation process, the fuel-to-nonfuel ratio, and the mixing characteristics, among other things. Taking into account the various uncertainties, it is still quite possible that fires would exist in the debris region and produce smoke in the aftermath of a nuclear attack. Thus, the debris region fires represent an important area of study.

Firestorms in particular are an important aspect of mass fires because of their potential impact on smoke transport to high altitudes. A firestorm may be defined as a stationary fire with an intense heat release and strong inflowing winds over a large area. Although the criteria necessary to initiate a firestorm are not well understood, two of the major factors seem to be that both the intensity and the extent of the fire must be quite large. For example, one of the 1943 Hamburg fires took about 2 hours to reach firestorm conditions over an urban area greater than 12 km^2. The heat intensity was on the order of 2.5×10^5 Wm^2 for more than six hours. While the present model does predict the heat release rate and area of urban fires, it does not predict the complicated interaction between the fires and fire-induced winds. Since firestorms probably develop by means of these interactions, more research is needed before reliable predictions of firestorms could be made. The convective storms that could be triggered by high fuel loads and high heat-release rates are discussed in Chapter 4.